eman ta zabal zazu

Universidad del País Vasco
Euskal Herriko Unibertsitatea

Mild Hyper-Excitation Induces Functional and Morphological Changes in Dendritic Spines in Mouse Brain Slices

Doctoral thesis

To obtain a doctoral degree

at the University of Basque Country

Author: Rizky Sarakhsi Ersaid Lasabuda

Supervisor: Jan Tønnesen

2024

(cc) 2024 Rizky Sarakhsi Ersaid Lasabuda (cc by-nc 4.0)

eman ta zabal zazu
Universidad del País Vasco
Euskal Herriko Unibertsitatea

NAZIOARTEKO
BIKAINTASUN
CAMPUSA
CAMPUS DE
EXCELENCIA
INTERNACIONAL

TESI ZUZENDARIAREN BAIMENA TESIA AURKEZTEKO	**AUTORIZACIÓN DEL/LA DIRECTORA/A DE TESIS PARA SU PRESENTACIÓN**

Zuzendariaren izen-abizenak /Nombre y apellidos del/la director/a: Jan Tønnesen

NIE: Y4970585T

Tesiaren izenburua / Título de la tesis: Mild hyper-excitation induces functional and morphological changes in dendritic spines in mouse brain slices

Doktorego programa / Programa de doctorado: Neurociencias

Doktoregaiaren izen-abizenak / Nombre y apellidos del/la doctorando/a: Rizky Sarakhsi Ersaid Lasabuda

Unibertsitateak horretarako jartzen duen tresnak emandako ANTZEKOTASUN TXOSTENA ikusita, baimena ematen dut goian aipatzen den tesia aurkez dadin, horretarako baldintza guztiak betetzen baititu.	Visto el INFORME DE SIMILITUD obtenido de la herramienta que a tal efecto pone a disposición la universidad, autorizo la presentación de la tesis doctoral arriba indicada, dado que reúne las condiciones necesarias para su defensa.

Tokia eta data / Lugar y fecha: Leioa, 13/05/2024

Sin. / Fdo.: Tesiaren zuzendaria / El/La director/a de la tesis

Universidad del País Vasco
Euskal Herriko Unibertsitatea

NAZIOARTEKO BIKAINTASUN CAMPUSA
CAMPUS DE EXCELENCIA INTERNACIONAL

AUTORIZACIÓN DE LA COMISIÓN ACADÉMICA DEL PROGRAMA DE DOCTORADO

La Comisión Académica del Programa de Doctorado Interuniversitario en **Neurociencias**, en reunión celebrada el día 14 de mayo de 2024, ha acordado dar la conformidad a la presentación de la Tesis Doctoral titulada: **Mild Hyper-Excitation Induces Functional and Morphological Changes in Dendritic Spines in Mouse Brain Slices**, dirigida por el Dr. **Jan Tønnesen** y presentada por D. **Rizky Sarakhsi Ersaid Lasabuda** adscrito al Departamento **Neurociencias**.

En Leioa a 14 de mayo de 2024

EL RESPONSABLE DEL PROGRAMA DE DOCTORADO

Fdo.: Prof. Dr. Pedro Grandes

eman ta zabal zazu
Universidad del País Vasco
Euskal Herriko Unibertsitatea
NAZIOARTEKO BIKAINTASUN CAMPUSA
CAMPUS DE EXCELENCIA INTERNACIONAL

AUTORIZACIÓN DEL DEPARTAMENTO

El Consejo del Departamento de Neurociencias, en reunión celebrada el día 15 de mayo de 2024, ha acordado dar la conformidad a la admisión a trámite de presentación de la Tesis Doctoral titulada:

“Mild HyperExcitation Induces Functional and Morphological Changes in Dendritic Spines in Mouse Brain Slices”

dirigida por el Dr. Jan Tonnesen y presentada por D. Rizky Sarakhsi Ersaid Lasabuda ante este Departamento.

En Leioa, a 15 de mayo de 2024

VºBº DIRECTOR/A DEL DEPARTAMENTO

Fdo: RAFAEL SARRIA AROSTEGUI

SECRETARIO/A DEL DEPARTAMENTO

Fdo: IZASKUN ELEZGARAI GABANTXO

ACTA DE GRADO DE DOCTOR O DOCTORA
ACTA DE DEFENSA DE TESIS DOCTORAL

DOCTORANDO/A DON/DÑA. ____

TITULO DE LA TESIS: ____

____

____

El Tribunal designado por la Comisión de Postgrado de la UPV/EHU para calificar la Tesis Doctoral arriba indicada y reunido en el día de la fecha, una vez efectuada la defensa por el/la doctorando/a y contestadas las objeciones y/o sugerencias que se le han formulado, ha otorgado por___________________la calificación de:

unanimidad ó mayoría

SOBRESALIENTE / NOTABLE / APROBADO / NO APTO

Idioma/s de defensa (en caso de más de un idioma, especificar porcentaje defendido en cada idioma):

Castellano ____

Euskera ____

Otros Idiomas (especificar cuál/cuales y porcentaje) ______________________________

En __________________a _____de ____________________de _____

EL/LA PRESIDENTE/A, EL/LA SECRETARIO/A,

Fdo.: Fdo.:

Dr/a: ____________________ Dr/a: ______________________

VOCAL 1º, VOCAL 2º, VOCAL 3º,

Fdo.: Fdo.: Fdo.:

Dr/a: _______________________Dr/a:__________________________Dr/a:_______________

EL/LA DOCTORANDO/A,

Fdo.: ________________________

This doctoral thesis was funded by a four-year scholarship from the Spanish Ministry of Science and Innovation's Predoctoral Training Program, awarded in November 2018 (FPI-MICINN, PRE2018-084210).

The experimental work has been financed by the following organizations:

- University of the Basque Country UPV/EHU (GIU21/048)
- Spanish Ministry of Science and Innovation (PID2020-113894RB-I00, PCI2022-135040-2)
- Aligning Science Across Parkinson's (ASAP), ASAP-020505
- Sigma XI grant in aid of research

Table of Contents

Abbreviations ... 15

Scope of This Thesis ... 9

Abstract ... 11

General Introduction ... 13

- The Synapse ... 13
- Neuronal adaptations: Synaptic plasticity and Intrinsic plasticity ... 16
- Dendritic Spine ... 17
- Hippocampal Anatomy ... 18
- Dendritic spines pathology ... 19
- Experimental model of dendritic spines: Epilepsy ... 20
- Research focus of the thesis ... 21

Hypothesis and Objectives ... 23

Materials and Methods ... 25

- Animals ... 25
- Acute slice preparations ... 25
- Electrophysiology ... 26
  - Patch clamp recordings ... 26
  - Cell-attached recordings ... 26
  - mEPSCs ... 26
  - Field recordings ... 27
- Pharmacological experiments ... 27
- Immunostaining ... 27
- Confocal Imaging ... 27
- Imaging spine dynamics ... 28
- Data Analysis and Statistics ... 28

Results ... 29

- Establishing a hyperexcitability model ... 29
- GABAergic inhibition increases cell firing activity ... 30
- Evaluating the intrinsic properties of CA1 neurons during neuronal hyperactivity ... 31
- Exploring the spine morphology following increased excitatory synaptic input ... 33
- Synaptic signaling during hyperexcitability ... 36

  Spatiotemporal analysis of spine morphological adaptation 38
Discussion 45
  Selecting GABAergic mechanism in CA1 pyramidal neurons as the primary manipulator 45
  Using PTX as the experimental model 45
  Evaluating intrinsic properties for insights into the functional dynamics of a neuron 45
  Neuronal hyperactivation induces spine morphological rearrangements 46
  Complex effects of PTX-mediated hyperexcitability in synaptic communication 47
  Unveiling electrophysiological insights and spine morphological alterations 48
  Exploring spine dynamics during PTX application 48
Future Direction 51
  Re-evaluation of findings using STED microscopy 51
  Astrocytic coverage during mild hyperexcitation condition 51
  Extracellular space 51
Conclusions 53
Collaborations 55
  Functional assessment of olfactory neuroepithelium cells in bipolar disorder patient 55
  Introduction 55
  Materials and Methods 56
    Cell Cultures 56
    Electrophysiology Recordings 56
    Data Analysis 56
  Results 57
    Olfactory neuro epithelium (ONE) cell intrinsic properties 57
  Discussion 59
  Conclusion 59
Acknowledgments 61
References 63

Abbreviations

AP : Action Potential

ACSF : Artificial Cerebro Spinal Fluid

CA1 : Cornu Ammonis 1

DAPI : 4′,6-diamidino-2-phenylindole

CC : Current Clamp

CNS : Central Nervous System

DG : Dentate Gyrus

DIC : Differential Interference Contrast

EC : Entorhinal Cortex

EPSCs : Excitatory Postsynaptic Currents

GABA : Gamma-aminobutyric acid

GFP : Green Fluorescence Protein

GFAP : Glial Fibrillary Acidic Protein

LEC : Lateral Entorhinal Cortex

MEC : Medial Entorhinal Cortex

mEPSC : Miniature Excitatory Postsynaptic Currents

PFA : Paraformaldehyde

PP : Perforant Path

PTX : Picrotoxin

RMP : Resting Membrane Potential

SB : Subiculum

SC : Schaffer Collateral

sEPSCs : Spontaneous Excitatory Synaptic Currents

STED : Stimulated Emission Depletion

Thy-1 : Thymus Cell Antigen 1

TLE : Temporal Lobe Epilepsy

TTX : Tetrodotoxin

VC **:** Voltage Clamp

WT : Wildtype

YFP : Yellow Fluorescent Protein

Scope of This Thesis

Dendritic spines are small protruding structures on the dendrites that receive synaptic inputs. Spines can change their morphology and number under various conditions, such as during learning and memory. Changes in shape and density have also been associated with numerous neurological disorders. So far, the explanation for such spines has been purely structural and within the context of synaptic plasticity or clinical manifestations. New insights from super-resolution studies view dendritic spines as an independent system that regulates signal transduction, specifically the magnitude of postsynaptic potential.

To better understand the abovementioned process, we used a modest acute hyperexcitability model. The general aim of this thesis is to shed light on neuronal adjustments induced by modest hyperexcitability, focusing on dendritic spine morphology that independently modulates synaptic function and its subsequent impact on synaptic signaling. Gaining more insight into this process, as generated and characterized in this thesis, will provide additional information needed for the fundamental biology of dendritic spines.

Abstract

The dynamic properties of dendritic spines are crucial for the modulation of synaptic strength and plasticity. While most experimental efforts have explored dendritic spines in response to specific events such as synaptic plasticity or in various neurological disorders, the potential role of structural spine neck changes in regulating neuronal function remains obscure. It appears likely that dendritic spines can independently regulate signal transduction, particularly the magnitude of postsynaptic potential, via its neck. Here, we induced modest hyperexcitation in mouse hippocampal slices using the GABAA receptor blocker picrotoxin (PTX) to identify the earliest functional adjustments in the hippocampal circuit. After 30 minutes of PTX treatment, we investigated the intrinsic membrane and dendritic spine structure in CA1 pyramidal neurons. Modest hyperexcitation, without sustained discharging, did not induce changes in intrinsic neuronal properties. However, we did observe subtle changes in dendritic spine shape that may impact signaling independently of synaptic release and post-synaptic receptor mechanisms. Our ongoing efforts will explore whether these changes reflect a beneficial homeostatic response to maintain the balance or contribute to a slow shift in the excitation/inhibition balance.

General Introduction

The human brain is a fascinating organ, essential for learning and memory. Rather than a mystery box, it actively encodes, retains, edits, and retrieves information based on experiences. These brain capacities enable us to understand, interpret, and adapt from unique perspectives. Our brain contains billions of neurons and forms a million new connections every second of our life. These dynamic features are widely regarded as the cellular foundation for our ability to learn and remember.

Although our genes provide a blueprint for the initial structure of brain circuits, their functional circuits are a subject of crucial relationships between biological structure and mind. This link is strengthened through repeated use and is tightly regulated by structural changes in synapses. Additionally, the morphological rearrangement of dendritic spines and functional remodeling of neurotransmitter receptors, such as AMPA receptors, plays a key role in facilitating these changes. However, many fundamental questions remain unanswered, such as how the dynamic morphology of dendritic spines affects electrical signaling in neurons. Given their crucial role in synapse function and synaptic plasticity, dendritic spine abnormalities have been implicated in several neurological disorders, such as intellectual disability and epilepsy.

The Synapse

To communicate with each other, neurons use specialized sites known as synapses, a concept pioneered by Ramón y Cajal over a century ago. Synapse formation and maintenance are tightly regulated processes, relying heavily on precise protein-protein interactions to ensure the proper signal transduction. Most synapses in the central nervous system (CNS) are chemical synapses that employ neurotransmitters, a chemical messenger, for signal transmission. Chemical synapses can then be classified based on their neurotransmitter: glutamatergic (excitatory signaling), GABAergic (inhibitory signaling), cholinergic, and adrenergic. Structurally, synapses comprise a presynaptic axonal terminal (or bouton) and a postsynaptic compartment, separated by a synaptic cleft **(Figure 1)**.

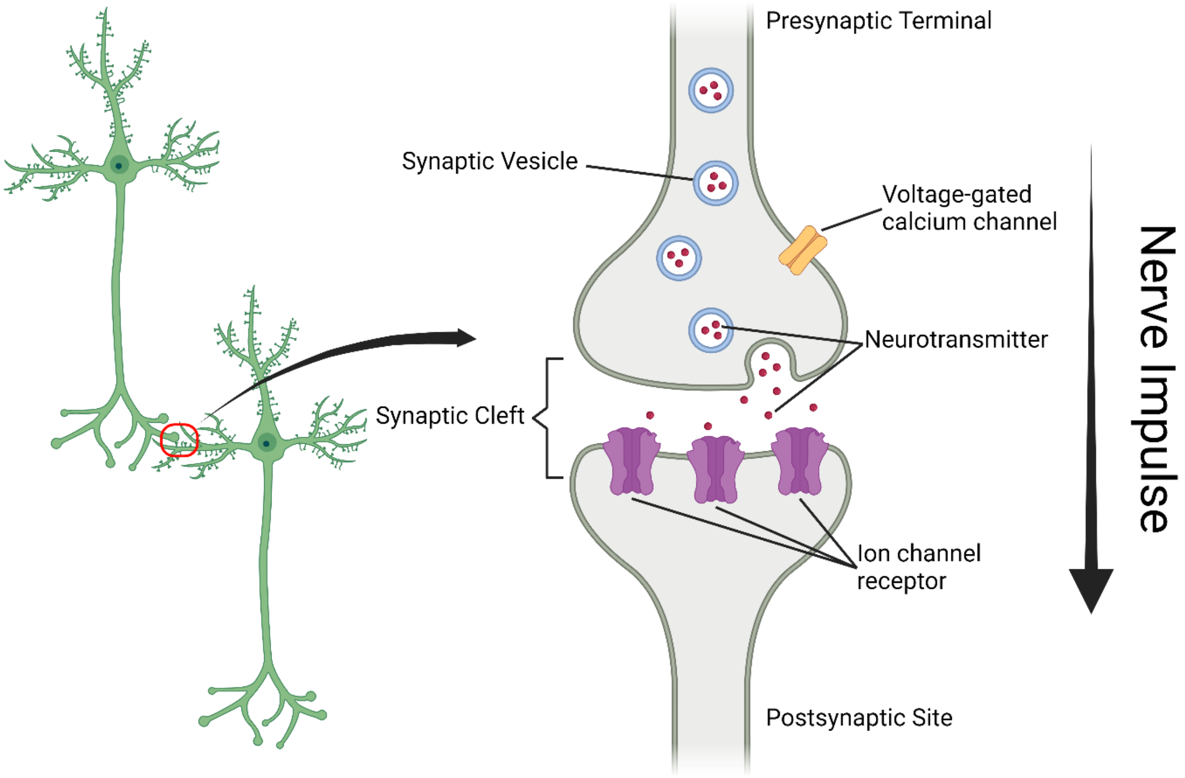
Presynaptic Terminal
Synaptic Vesicle
Voltage-gated calcium channel
Nerve Impulse
Neurotransmitter
Synaptic Cleft
Ion channel receptor
Postsynaptic Site

Figure 1. | Basic structure of a synapse. Neuron communicates through a synapse. The dendrites receive input signals from the neighbor's axon terminals. Right, a zoomed-in picture showing the main composition of presynaptic and postsynaptic compartments.

To convey synaptic signals, synaptic vesicles containing neurotransmitters in the presynaptic terminal are docked and primed for release in the active zone. When there is a stimulus, these readily releasable pools of synaptic vesicles release neurotransmitter that crosses the synaptic cleft (approx. 20 nm wide) to activate the corresponding receptors in the postsynaptic side (Zucker & Regehr, 2002). In the example of excitatory neurotransmission, glutamate interacts with α-amino-3-hydroxy-5-methyl-4-isoxazolepropionic acid (AMPA) or N-methyl-D-aspartate (NMDA) receptors. Subsequently, this would induce an excitatory postsynaptic potential (EPSP) by driving an influx of Na^+ that creates a transient depolarization. In contrast, gamma-aminobutyric acid (GABA), acting as an inhibitory neurotransmitter, induces an inhibitory postsynaptic potential (IPSP) by opening Cl^- channels in GABA receptors. This increase in negative ions or decrease in positive ions in the postsynaptic membrane reduces the likelihood of firing an action potential. Thereby, inhibitory synapses could fine-tune the quantity of action potential formation and refine the number of excitatory synapses.

An action potential is a condition where there is a rapid change in the voltage across a cellular membrane. It is widely thought that action potentials play an essential role in cell-cell communication. Neurons typically maintain a voltage difference, known as membrane potential, by using voltage-gated ion channels. These electrical properties allow neurons to generate an action potential or to be excited. Under no electrical impulses, these channels are closed due to the cell's resting potential, which is commonly measured at -70 mV. When there is a synaptic input, it can cause a temporary change in membrane potential by allowing an inward flow of sodium ions **(Figure 2)**. More positive ions in the electrochemical gradient, known as depolarization, cause the membrane potential to reach an action potential threshold (around -50 mV), which triggers more voltage-gated sodium channels to open. This rising phase reverses membrane polarity and reaches the peak of membrane potential (around +40 mV). It causes the inactivation of sodium channels and, in turn, activates potassium channels that allow efflux of K^+ ions, initiating the falling phase. Rapid repolarization of the membrane potential returns the electrochemical gradient to a negatively charged membrane potential. Due to the electrical properties of potassium channels, the outward flow of K^+ continues briefly and causes a transient negative potential exceeding its resting potential, known as afterhyperpolarization. This undershoots phenomenon ensures the action potential's unidirectional propagation and a positive feedback loop to restore the activation of the sodium pump. After several milliseconds, concentrations of Na^+ and K^+ return to their equilibrium, bringing the cell back to its resting membrane potential.

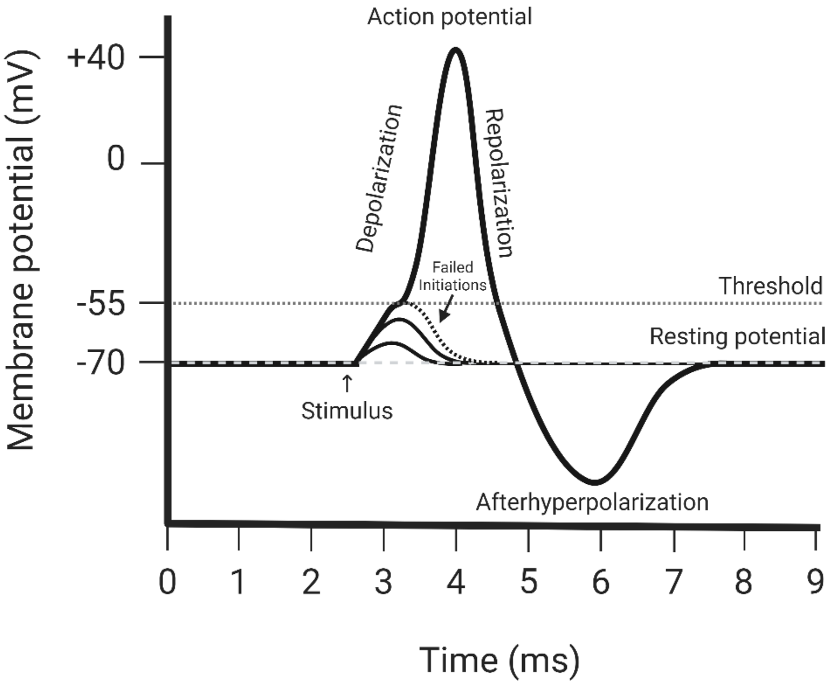

Figure 2. | Schematic representation of an action potential. Neuron typically has a resting membrane potential of approximately -70mV. A stimulus causes an influx of Na^+ and bring the membrane potential towards a positively charged membrane. If the synaptic input is sufficiently robust, it depolarizes the membrane potential beyond the threshold of −55 mV. Subsequently, the membrane potential rapidly ascends to a peak of +40 mV. Hyperpolarization starts immediately after an inactivation of Na^+ channel and release of K^+ that creates a rapid descent and overshoot to −90 mV. Finally, the membrane potential is restored back to its resting state of −70 mV.

Neuronal adaptations: Synaptic plasticity and Intrinsic plasticity

Neurons are naturally plastic, capable of regulating both synaptic strength and connectivity. Synaptic plasticity modulates synaptic capacity to strengthen or weaken their synaptic connections. Additionally, neurons can adjust their intrinsic excitability in response to new conditions and activity. Therefore, this plastic ability is widely believed to contribute to learning, memory, and other cognitive functions. Synaptic plasticity has several forms, categorized by duration, direction of change, mechanism, and induction protocols. Two prominent forms of synaptic plasticity are short-term plasticity and long-term plasticity.

Short-term plasticity (STP) involves temporary changes in synaptic strength and efficacy over relatively short periods, typically lasting seconds to minutes. This change can result in either synaptic facilitation, where the synaptic signal is strengthened, or synaptic depression, where it is weakened due to repeat stimulation within a short timeframe (Glickfeld & Scanziani, 2006). During synaptic facilitation, repeated signals cause an accumulation of calcium ions in the presynaptic terminal, increasing the neurotransmitter release probability and enhancing the postsynaptic response (Zucker & Regehr, 2002). In contrast, in synaptic depression, the rapid repetition of presynaptic stimulation depletes the readily releasable pool of synaptic vesicles, diminishing the presynaptic terminal's ability to transmit the synaptic signal. Altogether, these mechanisms are perceived as information processing, filtering out the repetitive or irrelevant signals (Hennig, 2013).

Long-term plasticity, unlike the short-term plasticity, lasts from minutes to hours or even longer (Bliss & Lømo, 1973). It is categorized into two types: long-term potentiation (LTP) and long-term depression (LTD). LTP and LTD are typically triggered by high-frequency and low-frequency stimulation, respectively. Compared to STP, long-term plasticity involves structural changes at the synapse, such as the expansion of dendritic spines in LTP. It also includes the trafficking of AMPA receptors in the postsynaptic membrane, all aimed at altering synaptic efficacy (Sumi & Harada, 2020). Chronic activation of AMPA receptors can later activate NMDA receptors and increase Ca^{2+} levels. High levels of Ca^{2+} subsequently activate Ca^{2+}-calmodulin-dependent kinase (CaMKII) and trigger more AMPA receptor insertion into the postsynaptic membrane (Goold & Nicoll, 2010). The interplay of these mechanisms is thereby considered to be the cellular basis of learning and memory.

From a network perspective, stronger connections with frequent interaction create solid relationships. To explain this event, Donald Hebb coined the term "neurons that fire together wire together" in the '40s. Subsequently, this group of neurons can recruit other neurons in a chain-reaction manner and continue to expand its network (Baer & Rinzel, 1991). As part of this complex system, neurons require self-regulation to avoid the recruitment process. Intrinsic plasticity, the ability of neurons to modify their intrinsic electrical properties, plays a central role in regulating the subthreshold of AP propagation, spike generation, and synaptic integration (Shim et al., 2018). This intrinsic neuronal property can either make synaptic plasticity more likely or, cut the recruitment process by slightly hyperpolarizing the neurons. As a proof of concept, an optogenetic approach to inhibit excessive hyperexcitability and epileptiform activity demonstrates this principle by selectively hyperpolarizing principal cortical neurons (Tønnesen et al., 2009). Thus, aberrations in intrinsic plasticity could produce hyperexcitable neurons capable of inducing seizures.

Another way neurons regulate network activity is through the exo- and endocytosis of AMPA receptors. While the number of NMDA receptors is relatively stable, the number of AMPA receptors could determine the fate of a synapse. Synaptic scaling, one form of homeostatic plasticity, is crucial for monitoring firing rates, adjusting the number of AMPA receptors, and scaling synapses to stabilize firing at synaptic sites (Turrigiano, 2012). Hence, synaptic scaling can compensate for increased or decreased overall input. For example, chronically heightened network activity, as seen in epileptic conditions, prompts the removal of AMPA receptors from synapses, whereas prolonged suppression increases the number of synaptic AMPA receptors (Goold & Nicoll, 2010). Accordingly, a synapse's tight regulation and temporal and spatial complexity make neurons highly vulnerable to changes.

Dendritic Spine

Among the several mechanisms to regulate the onset or magnitude of synaptic plasticity, dendritic spines have appeared to be one of the first immediate responses in synaptic plasticity (Grutzendler et al., 2002). Dendritic spines are membrane protrusions that form postsynaptic compartments and receive input at the excitatory synapses (Yuste & Bonhoeffer, 2001). Structurally, spines have a bulbous head, or spine head, and an elongated neck that connects to the shaft of the dendrite. They are typically categorized based on their anatomical size: stubby spines (similar head and neck width), mushroom spines (constricted neck and large bulbous head, >0.6 µm in diameter), and thin spines (long neck and small heads, <0.6 µm in diameter) (Peters & Kaiserman-Abramof, 1970). Mushroom and stubby spines are relatively stable, while thin spines are highly dynamic. Thin spines are also considered as the precursor of mature spines (Hotulainen & Hoogenraad, 2010). Spine morphology is believed to be crucial for synaptic function, given that spine head size correlates with synaptic strength and undergoes substantial alterations during synaptic plasticity (Tønnesen & Nägerl, 2016).

In general, the dendrites of a single neuron can have a variety of spine sizes, shapes, and densities depending on the cell type, age, localization, and disease state. Observations have shown that the number and morphology of spines can dictate the degree of neuronal connectivity and activity, respectively. Additionally, spine number and morphology can dynamically change in response to activity, with changes occurring within seconds to minutes (Attardo et al., 2015; Gu et al., 2014; Mizrahi et al., 2004; Pfeiffer et al., 2018). In an in vivo time-lapse imaging study of an epileptic model, a brief seizure lasting less than 5 minutes was observed to induce spine loss (Guo et al., 2012). In the hippocampus, spines have an average lifetime of 1-2 weeks, with a complete turnover of the entire synaptic population occurring within 4-6 weeks (Attardo et al., 2015) This spine turnover provides an anatomical site for forming additional neuronal contacts between neurons, which is necessary for enhancing synaptic transmission. In contrast, a reduction in spine number limits the possible contacts without involving axonal gain or loss (Fiala et al., 2002).

Even though there is a strong correlation between the spine head and synaptic strength, accumulating evidence shows the crucial role of the spine neck in compartmentalizing electrical signals as well as biochemical processes. (Araya et al., 2014; Jayant et al., 2017; Kwon et al., 2017; Tønnesen et al., 2014; Tønnesen & Nägerl, 2016). A study by Tønnesen et al., 2014, showed the effectiveness of the spine neck in modulating synaptic plasticity. Narrowed and constricted spine necks will have a more significant neck resistance, or Rneck, and thus can segregate high EPSPs in the spine head and dendrite. In contrast, spines with shorter and wider necks, resulting in a decrease in Rneck, will efficiently pass the synaptic input to the dendrite, making the relationship between input-output more predictable. Moreover, reduced Rneck can handle stronger synaptic currents as they can sustain the driving force, or the difference in electrical potential, even during repeated synaptic conductance increases. Hence, alterations in the spine neck may attenuate the synaptic input, functionally disinhibiting the synapse and contributing to the adjustment of synaptic integration.

Hippocampal Anatomy

The hippocampus serves as the ideal study model for understanding how dendritic spine adjustment occurs in response to neuronal activities. Hippocampal neurons mainly comprise pyramidal cells in the hippocampal subfields and granule cells in the dentate gyrus (DG). The dendrites of these principal neurons are covered with dendritic spines, which harbor the postsynaptic compartments of excitatory synapses. A pyramidal neuron innervates different layers of the hippocampus, stretching from stratum oriens, stratum pyramidale, stratum radiatum, and to stratum lacunosum moleculare (Perez-Cruz et al., 2011). Additionally, CA3 has an additional layer of stratum lucidum. Structurally, pyramidal neurons have a conically shaped soma, a single axon, apical dendrites, basal dendrites, and the presence of dendritic spines. In contrast to pyramidal cells, granule cells exhibit a mono-conical arbor of apical dendrites, characterized by all branches converging toward the superficial region of the molecular layer (Jones et al., 2003). This architecture of pyramidal cells allows the cells to receive synaptic inputs from different sources.

The hippocampus is part of the limbic system and plays a crucial role in memory activities, including short-term memory, long-term memory, and spatial memory (Holtmaat & Svoboda, 2009). During memory processing, the hippocampus receives significant input from layers 2 and 3 of the entorhinal cortex (EC), and it transmits its output to layers 5 and 6 of the EC (Witter et al., 2000). The hippocampal circuitry interconnects the EC with the dentate gyrus (DG) via the perforant path (PP). DG granule cells project mossy fibers to CA3 pyramidal neurons, forming Schaffer collateral (SC) projections to CA1 pyramidal neurons, which then project back to the EC **(Figure 3)**. Additionally, to receive and integrate synaptic input from CA3 and EC, CA1 hippocampal neurons receive excitatory input almost exclusively on dendritic spines. Given the close interdependence of the hippocampal circuit**,** it is, therefore, essential that the hippocampus maintains precise coordination and tight control over the principal cells.

To provide stability to the principal cell populations, inhibitory interneurons tune the responses of excitatory neurons. Hippocampal GABAergic inhibitory interneurons account for only 10-15% of the total population (Pelkey et al., 2017). Despite their low number in the local inhibitory circuit, GABAergic interneurons regulate the activation of cellular and circuit function through feedback and feed-forward inhibition (Kullmann, 2011). In the example of the CA1 region, GABAergic neurons densely wrap around the pyramidal cells and firmly control the proximal portion of apical dendrites (Papp et al., 2001). Nevertheless, some of the interneurons also connect to the apical tuft of apical dendrites (Ang et al., 2005).

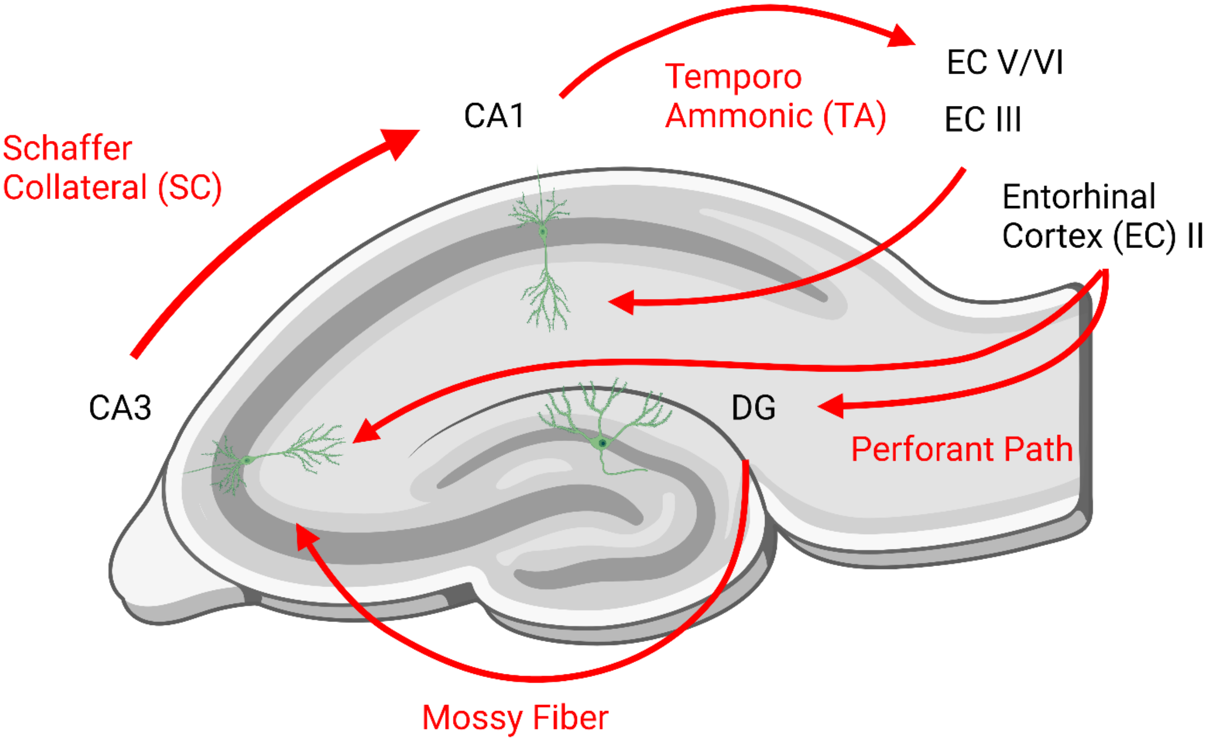

Figure 3. | Anatomical and functional connectivity of the hippocampus. The hippocampal neural circuit receives significant input from the entorhinal cortex layers 2 and 3 and delivers its output to layers 5 and 6 of the entorhinal cortex. Here, the information is processed sequentially. First, EC layer 2 projects into dentate gyrus (DG) granule cells through the perforant pathway (PP), then to CA3 pyramidal neurons through mossy fiber, onto CA1 via Schafer collateral (SC), and finally, CA1 pyramidal neurons send projections back to the EC layer 5.

Dendritic spines pathology

Dendritic spine abnormalities have been found in numerous neurodevelopmental, neuropsychiatric, and neurodegenerative disorders. Two main hallmarks of spine pathology are spine distribution and morphology. Changes in spine distribution represent dramatic increases or decreases in spine density. For example, permanent spine loss is common in ID cases and interestingly precedes the decreased number of neurons. Pathology of spine morphology involves distortions in spine shape and changes in spine size, which are also shown to be a response to various forms of neural injury. Even though spines are generally plastic and dynamic, these spine pathologies provide strong characteristics of a diseased brain.

With discoveries highlighting the crucial role of the spine neck in regulating biochemical and electrical signals, current research question aims to explore whether spine abnormalities are the underlying cause of neurological disorders. Several lines of evidence suggest that the appearance of spine pathology is not due to intrinsic pathologies of the neuron but rather a response of the spine to altered neuronal activities. Therefore, future detailed experiments are needed to determine the precise mechanisms by which dendritic spines control neurological disorders and compromise synaptic connectivity through spine pathology.

Experimental model of dendritic spines: Epilepsy

The dynamic process of establishing and refining synaptic connections between neurons is crucial for maintaining optimal brain function. Disturbance in this tight regulation could lead to various neurological and cognitive disorders. One example of this perturbation mechanism is epilepsy. Although many factors contribute to the development of epilepsy, in most cases, alterations in excitatory/inhibitory balance result in seizure generation. Epilepsy is one of the most common neurological disorders characterized by recurrent and unprovoked seizures (Falco-Walter, 2020). Among the different types of epilepsy, temporal lobe epilepsy (TLE) is one of the most severe, with a seizure focus typically located in the hippocampal area (Maillard et al., 2004).

To test our hypothesis that the spine neck can independently regulate synaptic efficiency, we considered the background theory behind epilepsy: neuronal hyperactivity. A disease model like epilepsy serves as the ideal model of network hyperexcitability. Since most excitatory synapses form at dendritic spines, in theory, increased neuronal activity could influence the synaptic structure and induce dendritic reorganization. Additionally, changes in dendritic spines can thus influence the synaptic strength and excitability of a neuron, misbalancing the excitatory/inhibitory nature of the neural circuit, and ultimately resulting in a hyperexcitable network seen in epilepsy (Becker, 2018; Martín-Suárez et al., 2023).

In vitro brain tissue preparations, especially in acute slices, offer a straightforward and accessible examination of simple brain networks. They are also suitable for high-throughput screening in a controlled and standardized environment. Several drugs with different action mechanisms have been used to induce hyperexcitable networks (Ergina et al., 2021; Velíšek, 2006; Zeng et al., 2007; Zha et al., 2005):

- $GABA_A$ receptor antagonists, such as Picrotoxin (PTX), Gabazine (Gbz), and Pentylenetetrazol (PTZ).
- Excitatory Amino Acid-related drugs (EAA) such as kainic acid (KA, an analog of L-glutamate) and 4-aminopyridine (4-AP; voltage-gated potassium channel blocker)
- Acetylcholine-related substances such as pilocarpine, which works as a muscarinic acetylcholine receptor agonist

Subsequently, typical changes that can provoke network excitability are regularly observed, including loss of inhibitory neurons (Martín-Suárez et al., 2023), intrinsic neuronal excitability (Smirnova et al., 2018), potentiation of excitatory synaptic contacts (Debanne et al., 2006), cell loss (Guo et al., 2012), and axonal sprouting (McKinney et al., 1997). Hence, experimental work to examine early spine adaptation in a modest hyperexcitation could support the notion that the dendritic spine could function as an independent synaptic regulator. However, future experiments are needed to determine and interpret this adaptive response. Is it a homeostatic response or a maladaptive one? Specifically, do these changes represent an effort to balance, or are they part of a harmful process?

Research focus of the thesis

Functional and morphological analysis of the immediate adaptations that are vital for neuronal function during hyperexcitability conditions will advance our understanding of how the healthy brain regulates cognitive processes. The aim of the research described in this thesis is to enrich our knowledge of the cellular mechanisms in the early stage of increased network activity, by elucidating the functional and structural implications during a modest induction of hyperexcitability. I particularly focus on the role of dendritic spines in regulating synaptic structure and function.

Hypothesis and Objectives

Dendritic spines serve as a vital excitatory post-synaptic element that plays a crucial role in neuronal communication. This essential feature is supported by their plastic ability to dynamically adjust their morphology. Furthermore, Tønnesen et al., 2014 highlighted the importance of the spine neck in regulating electrical signaling and biochemical diffusion, displaying its adaptability in response to synaptic activity.

On this basis, we seek to test the hypothesis that dendritic spines directly participate in regulating neuronal function. We speculate that heightened neuronal activity in the hippocampus will induce morphological changes, especially in the necks of dendritic spines, along with alterations in synaptic and intrinsic properties. Ultimately, these changes are expected to impact circuit excitability.

To comprehensively investigate this hypothesis, we will address two scientific objectives:

1. To assess the consequence of neuronal hyperactivity on cellular intrinsic properties and dendritic spines
2. To investigate the temporal progression of neuronal alterations following hyperexcitable events

These objectives will contribute to the current knowledge of whether changes in dendritic spines occur independently of synaptic plasticity and elucidate their potential effects on synaptic signaling.

Materials and Methods

Animals

All animal experiments were performed under guidelines from Spanish law (Real Decreto 53/2013, BOE 08-02-2013) and the European Communities Council Directive (2010/63/EU). These experimental works were accepted by the Animal Ethics Committee from the University of Basque Country (M20-2017-006, M20-2020-098). We used male wildtype C57BL/6J mouse (ENVIGO) and Thy1-YFP-H or B6.Cg-Tg(Thy1-YFP)HJrs/J (Jackson Laboratory) aged 4 to 12 weeks.

Acute slice preparations

Each mouse was decapitated, and the brain was then transferred into carbogenated (95% O2-5% CO2) ice-cold dissecting solution containing 195 mM Sucrose, 7 mM Glucose, 2.5 mM KCl, 1.25 mM NaH_2PO_4, 7 mM $MgCl_2$, 5 mM HEPES, 25 mM $NaHCO_3$, 1 mM Na-Ascorbate, 3 mM Na-Pyruvate, and 0.5 mM $CaCl_2$ (pH 7.2-7.3; 300-310 mOsm; All were purchased from Sigma -Aldrich). The brain was sectioned (350 µm) using a vibratome (Precisionary Compresstome VF-300) as described by Bischofberger et al., 2006 (**Figure 1**). The slices were then transferred into a carbogenated chamber of artificial cerebrospinal fluid (ACSF) containing 119 mM NaCl, 2.5 mM KCl, 1 mM NaH_2PO_4, 1.6 mM $MgCl_2$, 5 mM HEPES, 26 mM $NaHCO_3$, 10 mM Glucose, and 2.5 mM $CaCl_2$ (300-310 mOsm; pH 7.4) for at least 30 minutes at 37°C. After the recovery period, slices were incubated at room temperature for further use.

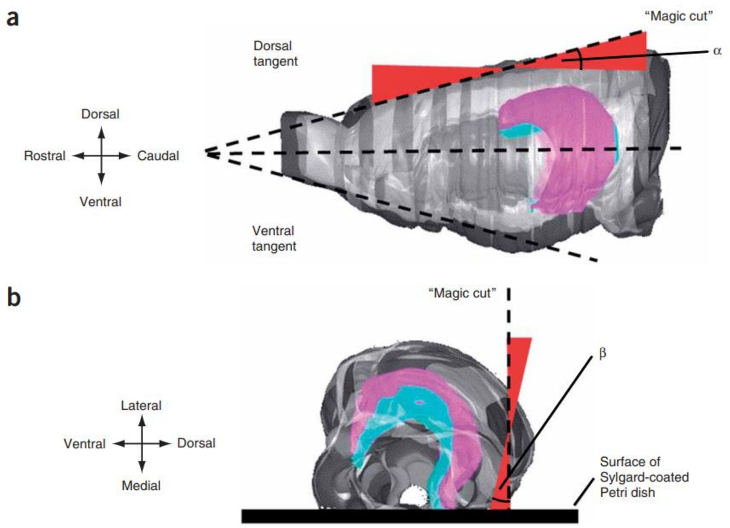

Figure 4 | Schematic illustration of the "magic cut" explained by Bischofberger et al, 2006. (A) View of the left hemisphere from top. Red sectors indicate the range of ''magic cut'. **(B)** View of the left hemisphere from the caudal. For CA1 pyramidal cell recording, α β of ~ 10° is preferable. Magenta indicates CA3 and CA1 regions; Cyan indicates dentate gyrus.

Electrophysiology

Slices were transferred into a flow recording chamber, held in place by a horseshoe-shaped platinum wire, and maintained at 35-37°C. The slices were perfused with carbogenated ACSF at a flow rate of 3.5 ml/min by a peristaltic pump.

Glass electrodes (3-6 MΩ) were pulled from borosilicate glass (Science Products Gmbh) with a vertical puller (PC-10, Narishige), fire polished, and backfilled with standard intracellular solution containing 125 mM K-Gluconate, 5 mM KCl, 10 mM HEPES, 1 mM EGTA, 4 mM Mg-ATP, 0.3 mM Na_2-GTP, 10 mM NaP-Creatine, and 3 mM Ascorbic Acid and 2.68 mM biocytin for subsequent experiments on spine morphology. The region of interest (ROI) was located using a 4x lens objective, and the individual cell was observed using a 60x immersion objective with infrared differential interference contrast (DIC) light (CleverExlore, MCI Neuroscience). The electrophysiological recordings were made using a HEKA EPC10 double amplifier and controlled with HEKA Fitmaster Software. The electrophysiological data was sampled at 10 kHz.

Patch clamp recordings

After the formation of a Giga-seal, the attached cell was ruptured, and whole-cell recordings were performed. The cell was clamped at -70mV, and the recordings were made after 2 minutes to ensure the steady state of the cells. Seals with a series resistance greater than 25 mΩ were rejected, and the capacitance compensation was performed automatically. The cellular intrinsic properties were assessed from the voltage response by the current step protocol from -100 pA to 280 pA in 20 pA increments and 900 ms duration. Only neurons with typical pyramidal morphology were included. Ramp injection of 0-500 pA over 1s was used to determine the excitability of the cells, including the rheobase, slope, and action potential threshold. The resting membrane potential (RMP) was calculated as the averaged membrane potential 100 ms before the current ramp injections.

Cell-attached recordings

To evaluate the synaptic potential activity, cell-attached recording was performed. While approaching the cell, positive pressure was applied to the tip electrode. The gigaseal was obtained by adding additional suction to the electrode. The cell membrane was not ruptured and maintained at 0pA holding current during this gigaseal-attachment. Each cell was recorded in a current clamp continuous mode for 35 minutes.

mEPSCs

Miniature EPSCs (mEPSCs) were recorded in whole-cell voltage clamp mode at -70 mV in the presence of 0.5 mM tetrodotoxin (TTX; Abcam). The amplitudes were determined from the baseline to the peak. Only amplitude that has >15 pA is included in the analysis.

Field recordings

To verify our study model, field recordings in the CA1 region were performed using fire-polished glass capillaries (1-2 MΩ) backfilled with ACSF. The cell activity was recorded over a span of 50 minutes with continuous current clamp recording at 0 pA.

Pharmacological experiments

To induce neuronal hyperactivity in vitro, 100 µM Picrotoxin (PTX; Abcam) was added to the perfusion ACSF. PTX is a $GABA_A$ blocker. After baseline recording for the control group, slices were then incubated in this solution for 30 minutes and labeled as a treated group **(Figure 2)**.

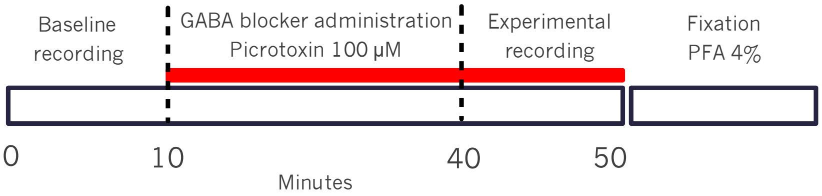

Figure 5 | Experimental timeline for the electrophysiology recording. First, the slice was perfused with ACSF to establish a baseline condition. Next, a mixture of ACSF + PTX 100 µM was added to induce neuronal overactivation and perfused for 30 minutes. After the incubation period, cells were recorded to observe the effect of PTX. If there were no crucial changes in series resistance, slices were then followed by a 1-hour perfusion with 4% PFA for an Immunostaining.

Immunostaining

After the electrophysiological recording, slices were fixed in a PFA solution (4% paraformaldehyde) for at least 1 hour on a plate shaker at room temperature. Slices were then stored in PBS for subsequent experiments.

To detect the biocytin and label the astrocytes, immunostaining on free-floating sections was performed following the protocol described by Swietek et al., 2016. Slices were washed three times in PBS for 10 minutes and permeabilized using 0.3% Triton X-100 (Alfa Aesar) in PBS solution for 30 minutes. The slices were then washed in PBS before being blocked overnight at 4°C with a blocking buffer containing PBS, 0.3% Triton X-100, and 4% horse serum (GIBCO). The following day, the primary antibody, anti-GFAP (Rabbit, Abcam AB7260, 1:1000), dissolved in the blocking buffer, was added to the brain sections. The slices were then incubated overnight at 4°C. The slices were rinsed eight times with 0.3% Triton X-100 in PBS for 15 minutes and then stained with the secondary antibody: Goat anti-Rabbit IgG H&L (Cy3, Abcam AB97075, 1:1000) and Streptavidin (FITC, Abcam AB13621, 1:1000) for 3 hours at room temperature. Following two rinses with 0.3% Triton X-100 in PBS and two rinses of PBS for 15 minutes, slices were mounted on glass slides using Fluoroshield Mounting Medium with DAPI (Abcam Ab104139).

Confocal Imaging

The labeled brain slices were imaged by Ricardo Andrade using a confocal microscope (LSM 880, Fast Airyscan, Zeiss) with the Z-stack function. For an overview of the cells, the biocytin-positive neurons were imaged with a 10x objective and digital zoom of 1.5x, while for their dendrites, a 63x objective with a digital zoom of 3x was used. The cells were then imaged to extract two regions of interest: the apical and basal layers, which included the primary and secondary dendrites for further analysis.

Imaging spine dynamics

All images for the spine dynamics experiment were acquired using a two-photon Femtonics 2D upright microscope (Olympus BX61 WI). To identify the hippocampal CA1 region, we used a 4X Olympus objective. For image acquisition, we utilized a 20x water immersion Olympus objective with a zoom factor of 6.0534, which was equipped with a Spectra-Physics MAI THAI (HPDS-007) laser and taken at 905nm.

To track dendritic spine dynamics, spines were imaged for 35 minutes with intervals of 7 minutes (flow rate 2.5 mL/min). Each fluorescent image consisted of z-stacks with 11 steps at intervals of 0.5 µm. Image acquisition settings were set to 1000 pixels and an average of 3x. A representative healthy dendrite and an adequate number of spines were essential.

Data Analysis and Statistics

Electrophysiological recordings were analyzed using FitMaster (HEKA Electronics), IGOR Pro 6 (Wavemetrics), Clampfit (Molecular Devices), and Nest-O-Patch (Dr. V. Nesterov). Each recording trace and its analysis results were visualized using Graphpad.

Miniature events were automatically detected and analyzed using Clampfit 10 software (Molecular Devices). However, only events that have amplitude >15 pA were accepted.

Images from airyscan confocal microscopy were analyzed using FIJI/imageJ software. The Z-stacked images were stacked to generate a maximum projection image. Each ROI was then further analyzed using the Spine J plugin (Levet et al., 2020)For this nano-structural analysis, four parameters—spine length, spine neck length, head area, and spine density—were obtained.

Statistical analyses were performed using GraphPad Prism version 8.0. Non-parametric two-sided statistical tests (Wilcoxon signed-rank, Mann–Whitney U, and Kruskal–Wallis ANOVA tests) were used to avoid assumptions of normality in time-lapsed imaging experiments. A mixed-effects statistical model was also utilized to account for variability due to random effects. Frequency distributions were binned accordingly, as specified throughout, and a log-normal curve fit was applied to the histogram. Other specific tests used are reported in the captions of the figures.

Results

Establishing a hyperexcitability model

Numerous epileptic models have been developed using different pharmacological approaches. Given that the objective here is to select suitable drugs to induce hyperactivity, we conducted an exhaustive literature study. A previous study by Hablitz in 1984 described that picrotoxin (PTX), a $GABA_A$ antagonist, can cause epileptiform activity in vitro (Hablitz, 1984). This effect of PTX on developing seizure-like activity is thought to occur through the excitatory/inhibitory synaptic imbalance. Here, we investigated the direct effect of 100 µM PTX on the network level of CA1 hippocampal neurons in acute slices using field potential recordings. Only neurons from juvenile mice aged 6-11 weeks were used to minimize developmental variability. Likewise, the frequency of spontaneous activity after 30 minutes of PTX application was significantly increased **(Figure 6)**. Therefore, this experiment validates the use of PTX as our hyperexcitability model.

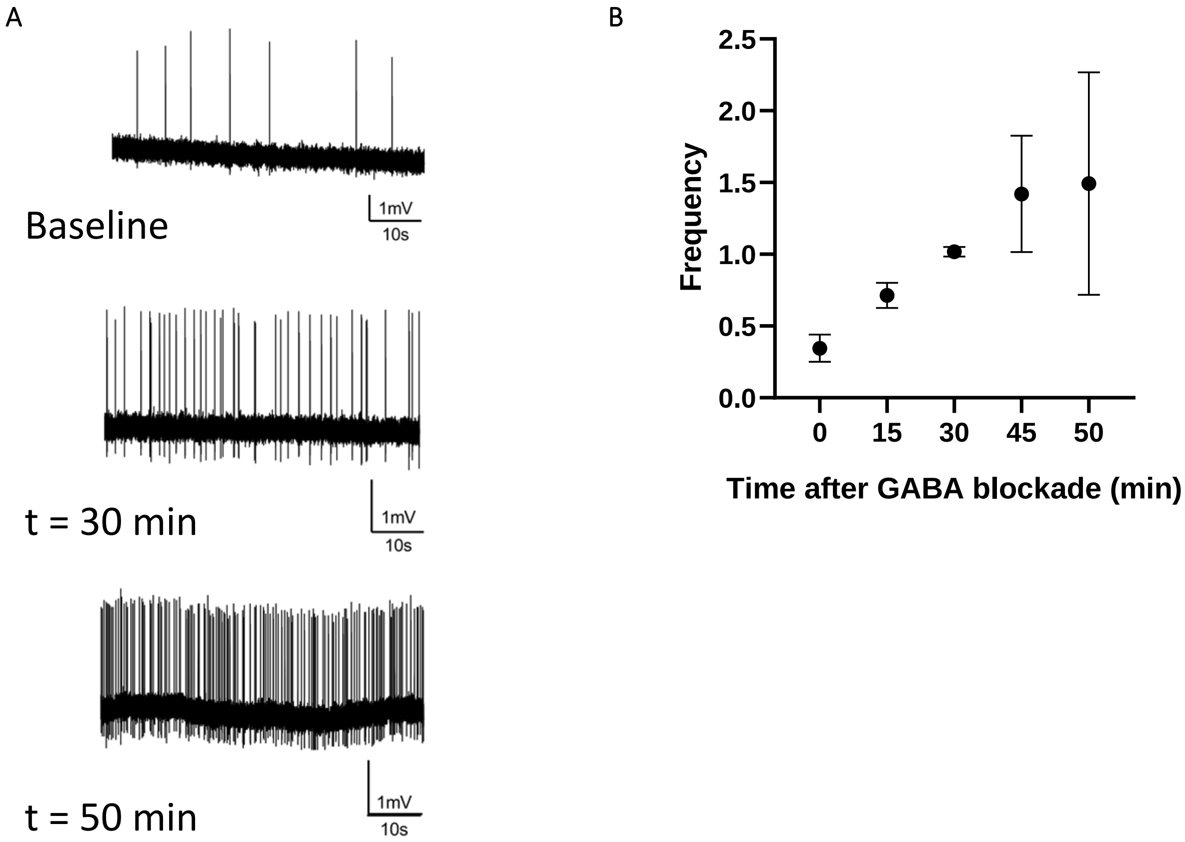

Figure 6. | Example of representative traces of field potentials recording with spontaneous activity. **(A)** Baseline, top. After 30 minutes, middle. After 50 minutes, below. **(B)** Average frequency of spontaneous activity during continuous current clamp recording at 0 pA. n = 3 neurons from 3 animals.

GABAergic inhibition increases cell firing activity

To further verify whether the brief application of PTX could induce hyperexcitation activity in acute slices of CA1 hippocampal neurons, we performed a cell-attached recording. This technique is suitable for recording cell-firing activity as it does not require cell rupture, and the recorded activity is in the form of action potential currents (APs). Results showed a significant increment in the number of APs during the PTX administration compared to the control (Control 2.375 ± 5.95 and PTX 520.571 ± 632.44, $p<0.001$, D = 0.7619, Kolmogorov-Smirnov test) **(Figure 7)**.

Taken together, our results demonstrate that 30-minute exposure to a bath application of 100 µM PTX reliably enhances excitatory transmission within the network. This finding also suggests the possibility of functional changes in neuronal behavior induced by an imbalance in excitation/inhibition. Ultimately, our results not only corroborate our experimental model but also support our research proposal, which aims to detect changes in intrinsic properties and dendritic spines as early as possible following neuronal hyperactivity.

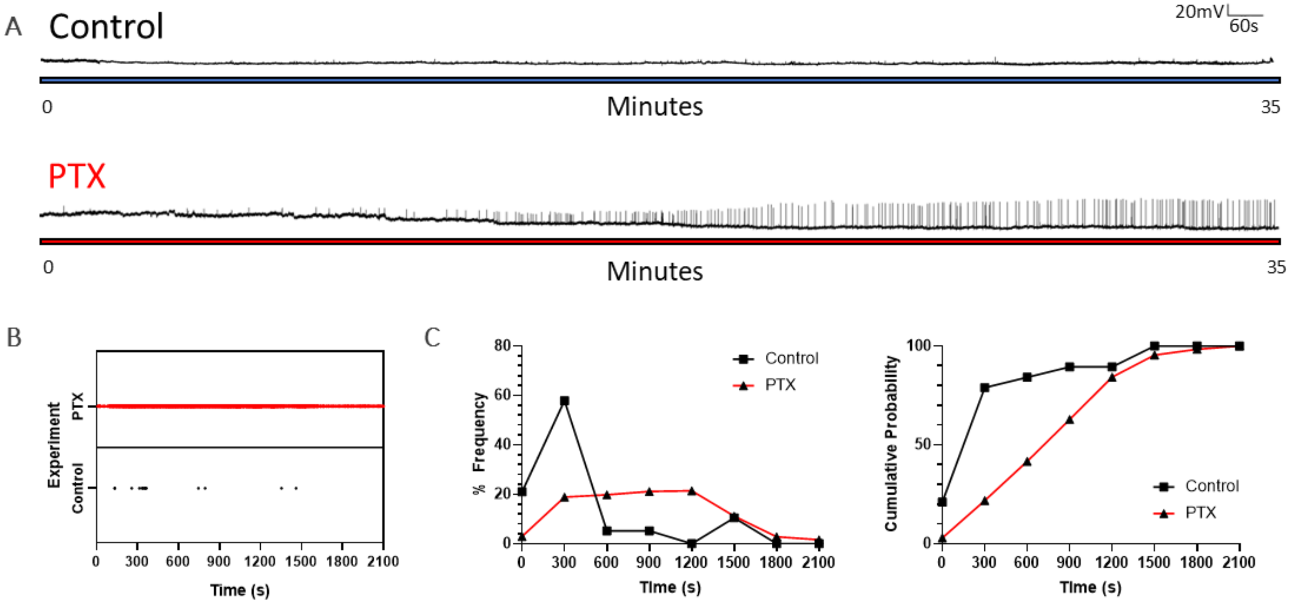

Figure 7. | PTX application increases cell firing activity in CA1 hippocampal slices. (A) Example traces from cell attached recordings in control (above) and in the presence of PTX (below). **(B)** The number of APs during the recording were converted into a raster plot. n = 8 slices, 8 animals for control; n = 7 slices, 7 animals for PTX group. **(C)** Distribution curves and **(D)** Cumulative distribution of APs in control and PTX binned per 5 minutes. A significant difference between control and PTX ($p<0.0001$, D = 0.7619) was detected with the Kolmogorov-Smirnov test.

Evaluating the intrinsic properties of CA1 neurons during neuronal hyperactivity

To explore possible changes in the intrinsic properties of CA1 pyramidal neurons, we conducted patch-clamp recordings in acute hippocampal slices. We evaluated the resting membrane potential (RMP) and threshold potential from 11 neurons in control group and 7 neurons from treated group (N= 17 animals). No differences in RMP recorded at 0 pA **(Figure 8B)**. A similar situation was observed in the potential threshold following PTX administration (**Figure 8C**). Interestingly, at the threshold depolarization, neurons treated with PTX fired more action potentials (Control 1.444 ± 0.24 and PTX 2.444 ± 0.38, $p<0.05$, Paired T-Test). Thus, a brief hyperexcitation condition is very likely to promote an increase in synaptic firing (**Figure 8D**). Nevertheless, gross AP in the entire course of the current step protocol showed no significant difference (**Figure 8E**).

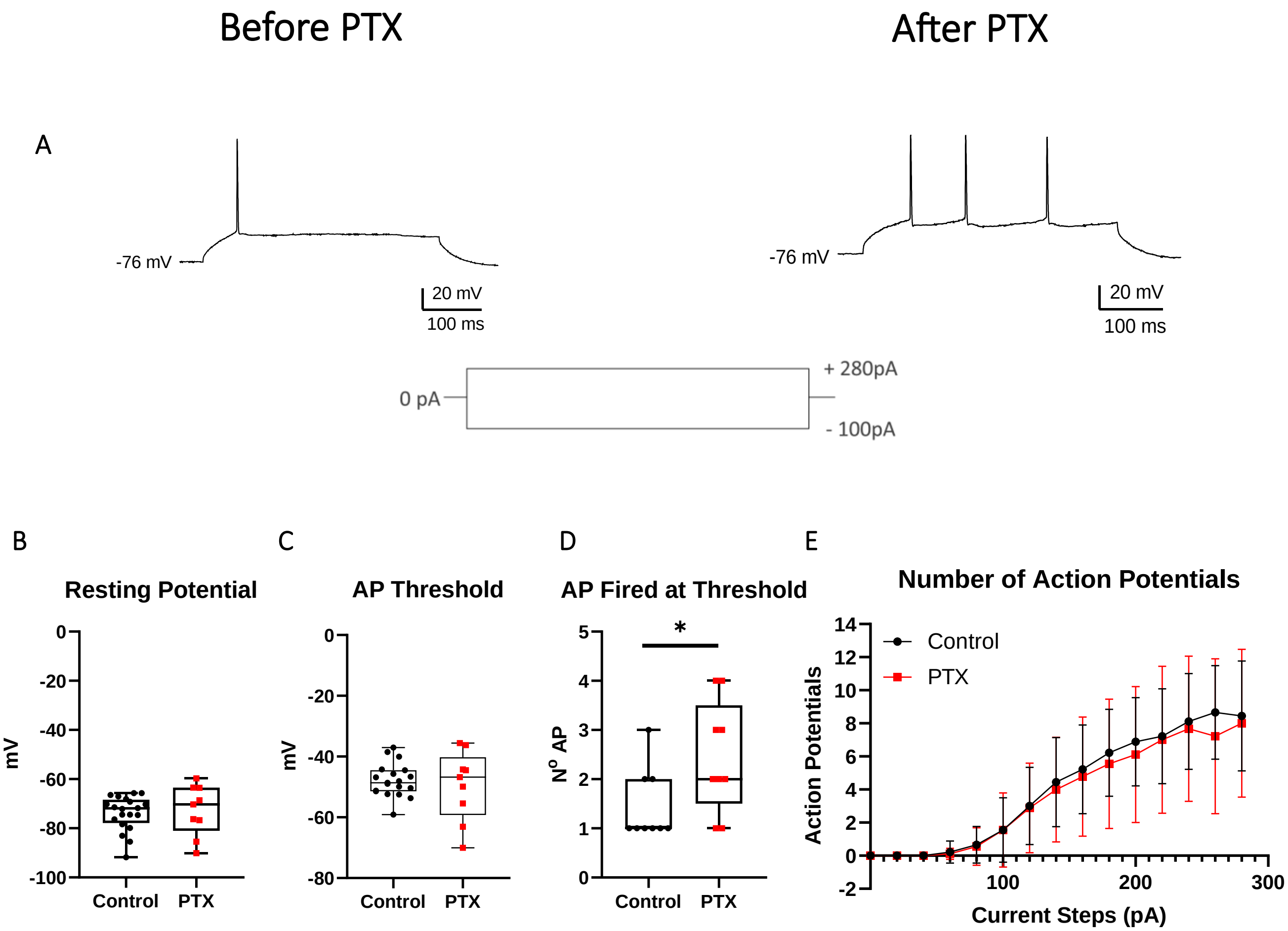

Figure 8. | Intrinsic properties and homeostatic responses before and after PTX application. (A) Representative voltage responses from before (left) and after (right) PTX application of CA1 pyramidal neurons. Current clamp step injection (Istep) protocol, from -100 pA to 280 pA in 20 sweeps. Below is the cartoon of Istep protocol. **(B)** Distribution of resting membrane potential (RMP) of individual neurons at 0 pA. **(C)** Threshold potential. **(D)** Quantification of AP fired in the excitation threshold. **(E)** Current clamp step protocol (Istep) and the number of AP relationships. n = 11 neurons from 10 animals for control; n = 7 neurons from 7 animals for treated. Statistical analysis was performed with a paired t-test. * $p<0.05$.

To further investigate the neuronal excitability, we analyzed input resistance, rheobase, and slope using a depolarizing ramp current injection protocol. For this, we injected a current ramp from 0 pA to 500 pA over 1 second. As shown in the example trace, CA1 pyramidal neurons treated with PTX displayed a prominent difference in response **(Figure 9A)**. However, there were no significant differences in input resistance, rheobase, and slope analysis (**Figure 9B-E).** Collectively, the quantification of APs fired during this ramp protocol is similar **(Figure 9E)**. Taken together, these results confirm that the intrinsic properties of the cell remain preserved during the neuronal overactivation.

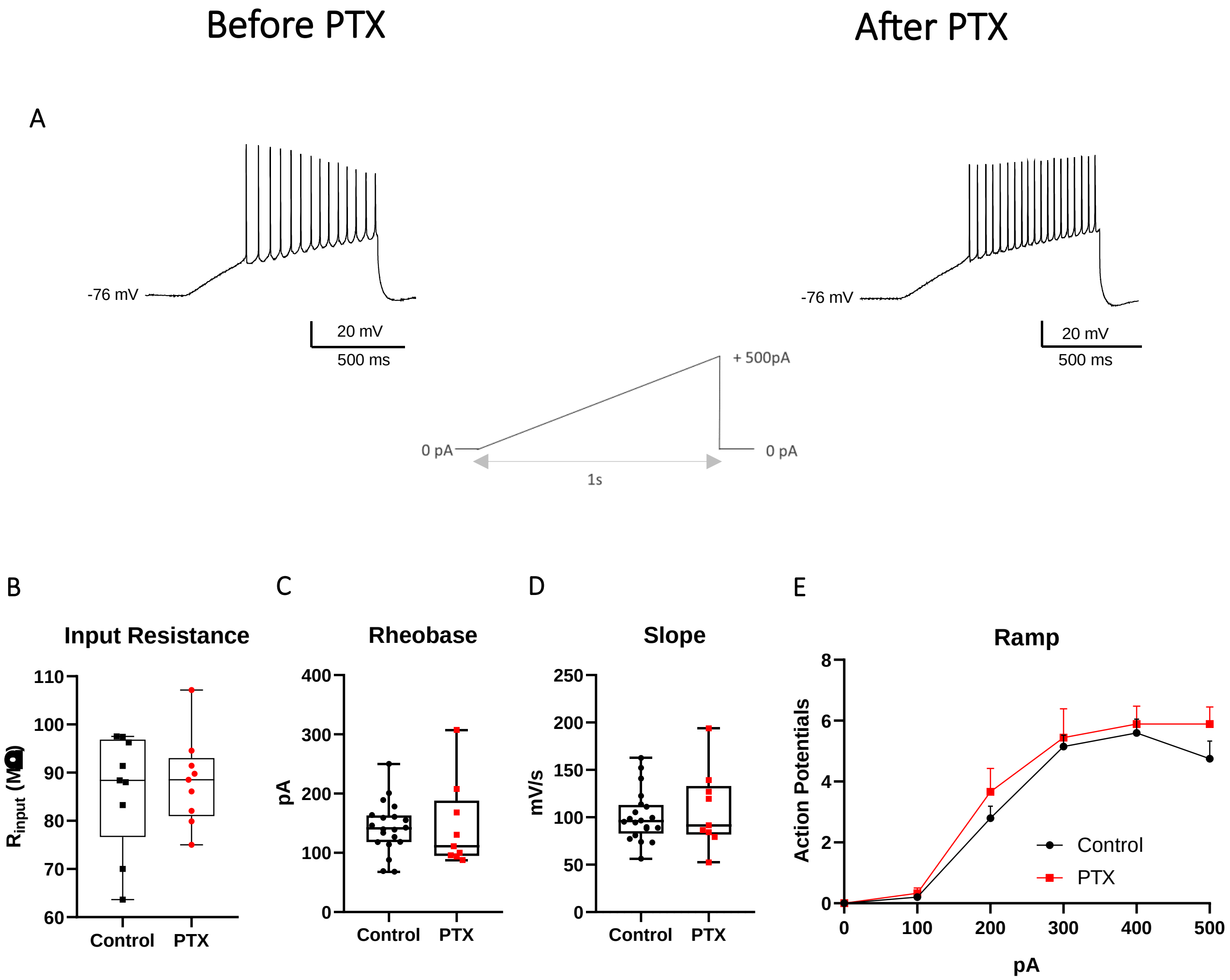

Figure 9. | Firing properties of CA1 remains unchanged upon PTX application. (A) Example trace of voltage response upon ramp current protocol from 0 pA to 500 pA in 1s before (left) and after (right) PTX administration. **(B-E)** Analysis of the ramp injections. **(B)** Input resistance. **(C)** Rheobase. **(D)** Slope. **(E)** Count of AP fired during the current ramp protocol.

Exploring the spine morphology following increased excitatory synaptic input

To investigate the effect of excessive neuronal activity on dendritic spines, the patched cell was loaded with biocytin and labeled using immunohistochemistry techniques. The stained acute slices were then imaged using Airyscan confocal microscopy to visualize dendritic spines.

For standardized and unbiased counting and measurement of spines, we used Spine-J analysis (Levet et al, 2019). This semi-automatic ImageJ plugin is capable of measuring nanoscale structural details, including spine necks. This feature will enable us to evaluate further the direct correlation between spine necks and neuronal hyperactivity. As can be seen in **Figure 10**, Spine-J was able to detect and automatically measure dendritic spines.

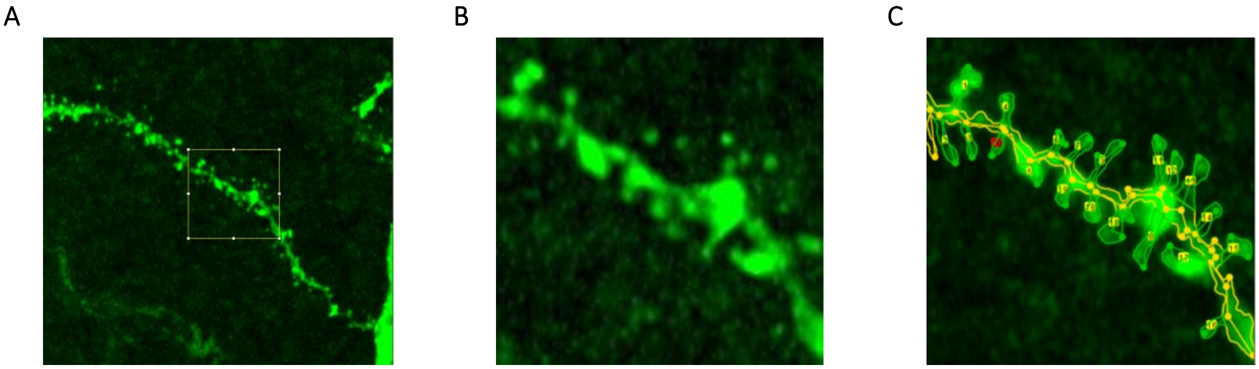

Figure 10. | Spine analysis at 63x magnification using SpineJ analysis. (A) Overview of a dendrite. **(B)** Part of the dendrite before and **(C)** after spine analysis. Overall, the Spine-J analysis gives more comprehensive analysis and reliable results

To better understand the spine morphological adaptations, we distinguished between apical and basal dendrites. This differentiation is mainly based on their anatomical location, the source of synaptic inputs, and their roles in information processing (Klausberger & Somogyi, 2008; Spruston, 2008). In addition to the apical dendrite analysis, we also discriminated between secondary and tertiary apical dendrites. Here, we anticipated potential differences in outcomes due to factors such as distance from the soma and the role of additional sites for synaptic contact, which could play crucial roles in mediating neuronal hyperactivity (Papp et al., 2001). In order to have a complete assessment of spine structure, we measured spine length, spine neck length, head area, and spine density.

In secondary apical dendrites, we analyzed 342 spines (n= 6 cells) in treated cells and 598 spines (n= 8 cells) in control neurons. **(Figure 11A)**. The mean spine length after GABAergic disinhibition (0.71 ± 0.02 µm) was lower than in control (0.83 ± 0.02 µm; p< 0.001; **Figure 11B**). The mean spine neck length was also shorter (0.41 ± 0.02 µm) than in control neurons (0.51 ± 0.01 µm; p< 0.001; **Figure 11C**). Indeed, the cumulative distribution plots for spine length and spine neck length were shifted toward the left **(Figure 11F & 11G)**. In terms of the spine head size, the mean head area was smaller in the treated group (0.081 ± 0.003 µm2) versus in the control (0.089 ± 0.002 µm^2; p< 0.001; **Figure 11D**). Accordingly, a similar trend of the cumulative distribution plot as spine length and spine neck length was observed **(Figure 11H)**. There was no difference in spine density between treated cells (1.94 ± 0.14 spines/µm; n = 15 segments, total length of dendrite 196.075 µm) and the control group (2.13 ± 0.11 spines/µm; n = 21 segments, total length of dendrite 276.621 µm; **Figure 11E**). Altogether, mild hyperexcitation condition induces a high degree of spine modification in secondary apical dendrites.

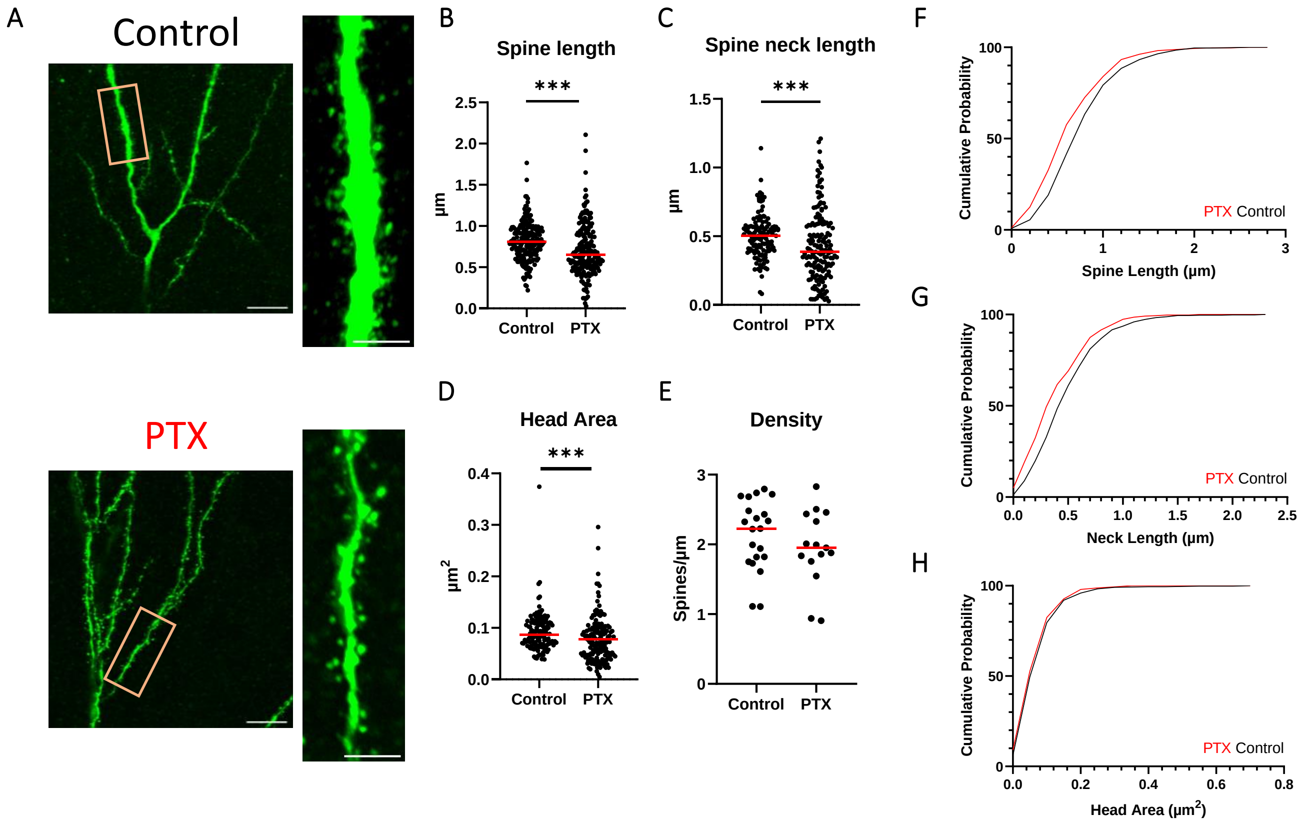

Figure 11. | Spine analysis of secondary apical dendrites. (A) CA1 Pyramidal neurons loaded with biocytin in control (above) and treated group (below). **(B-E)** Analysis of SpineJ software resulting in 4 spine parameters: **(B)** spine length, **(C)** spine neck length, **(D)** head area, and **(E)** spine density. Cumulative distribution of apparent spine length **(F)**, spine neck length **(G)**, and head area **(H)**. n = 598 spines in 196.075 µm dendrite from 8 neurons (8 animals) for control; n = 342 spines in 276.621 µm from 6 neurons (6 animals) for treated group were analysed. Statistical analysis was performed with Mann-Whitney-U test. *** P < 0.001. Shown is median. Scale bar 10 µm for overview & 3 µm for the zoomed part.

In the tertiary dendrites, we assessed 602 spines from 6 cells in treated cells and 444 spines from 8 cells in control neurons. As depicted in **Figure 12**, no significant differences were observed in all parameters. This includes the spine length (0.77 ± 0.02 µm), spine neck length (0.46 ± 0.01 µm), spine head area (0.091 ± 0.002 µm^2), spine density (2.30 ± 0.08 spines/µm; n = 19 segments, total length of dendrite 257.162 µm) in treated cells versus spine length (0.74 ± 0.02 µm), spine neck length (0.45 ± 0.01 µm), spine head area (0.087 ± 0.004 µm^2), and spine density in control (2.54 ± 0.12 spines/µm; n = 15 segments, total length of dendrite 180.329 µm), respectively. Therefore, these results indicate that spine morphology in tertiary dendrites remained stable amidst neuronal hyperactivity.

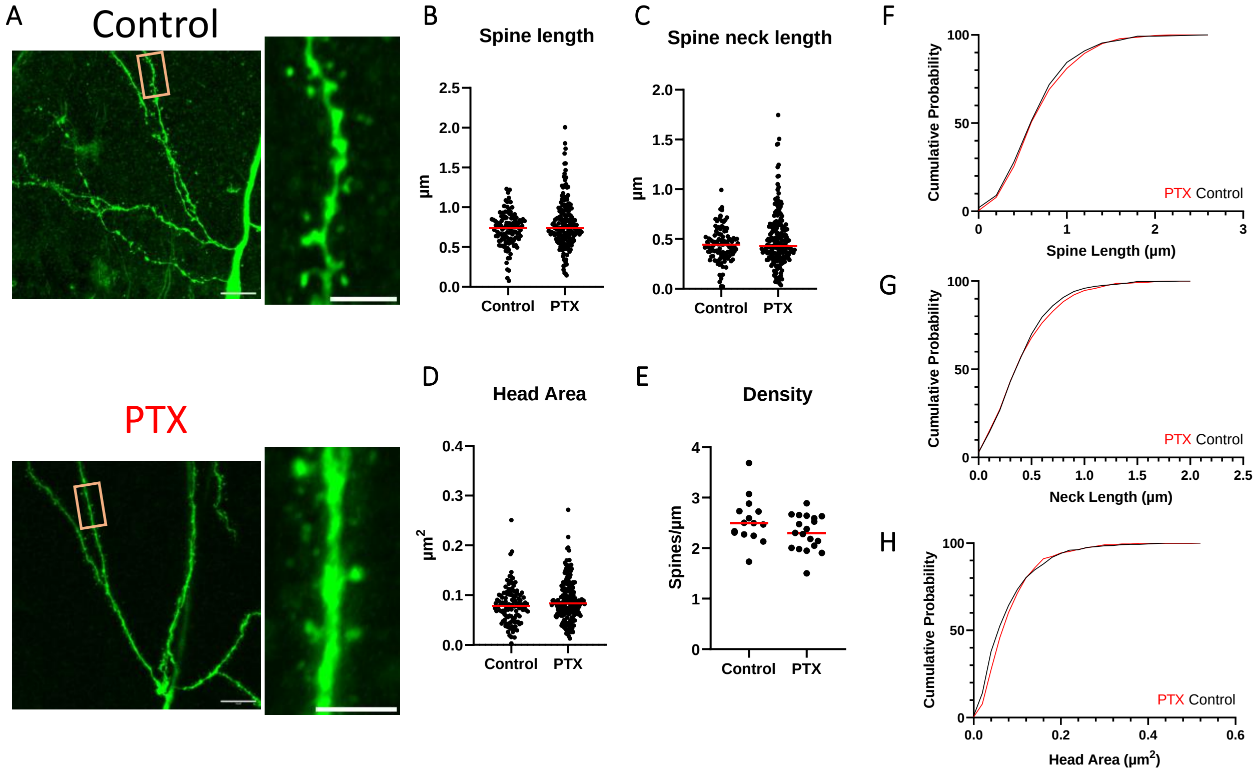

Figure 12 | Spine analysis on tertiary apical dendrites. (A) Representative confocal image showing acute dendritic spines in control (above) and treated neurons (below). Quantification of **(B)** spine length, **(C)** spine neck length, **(D)** head area, and **(E)** density**.** Cumulative probability of **(F)** spine length, **(G)** spine neck length, and **(H)** head area. Analysis involved n = 444 spines in 180.329 µm dendrite from 8 neurons (8 animals) for control; n = 602 spines in 257.162 µm from 6 neurons (6 animals) for treated group. Statistical analysis was performed with Mann-Whitney-U test. *** $P < 0.001$. Shown is median. Scale bar: 10 µm for overview and 3 µm for the zoomed part.

A similar analysis to the one performed in apical dendrites was applied to basal dendrites. We analyzed 918 spines in treated neurons and 1037 spines in control neurons. Of these, we found no difference in the mean spine length after PTX administration (0.69 ± 0.01 µm) compared to control (0.71 ± 0.01 µm; **Figure 13B**). Intriguingly, the spine neck length was longer in treated neurons (0.46 ± 0.01 µm) than in control (0.42 ± 0.01 µm; $p< 0.001$; **Figure 13C**), while the treated neurons displayed significantly smaller spine head area (0.038 ± 0.002 µm^2) compared to control (0.082 ± 0.002 µm2; $p< 0.001$; **Figure 13D**). Additionally, there was no detectable difference in spine density between treated neurons (3.57 ± 0.36 spines/µm; n = 22 segments; total length of dendrite 382.62 µm) and control neurons (2.367 ± 0.28 spines/µm; n = 35 segments, total length of dendrite 329.88 µm; **Figure 13E**). Quantitatively, the cumulative distributions of morphological parameters complemented our analysis of spine measurements (**Figure 13F-H).** These results suggest that increased neuronal activity favors a smaller head area and longer spine neck length in basal dendrites.

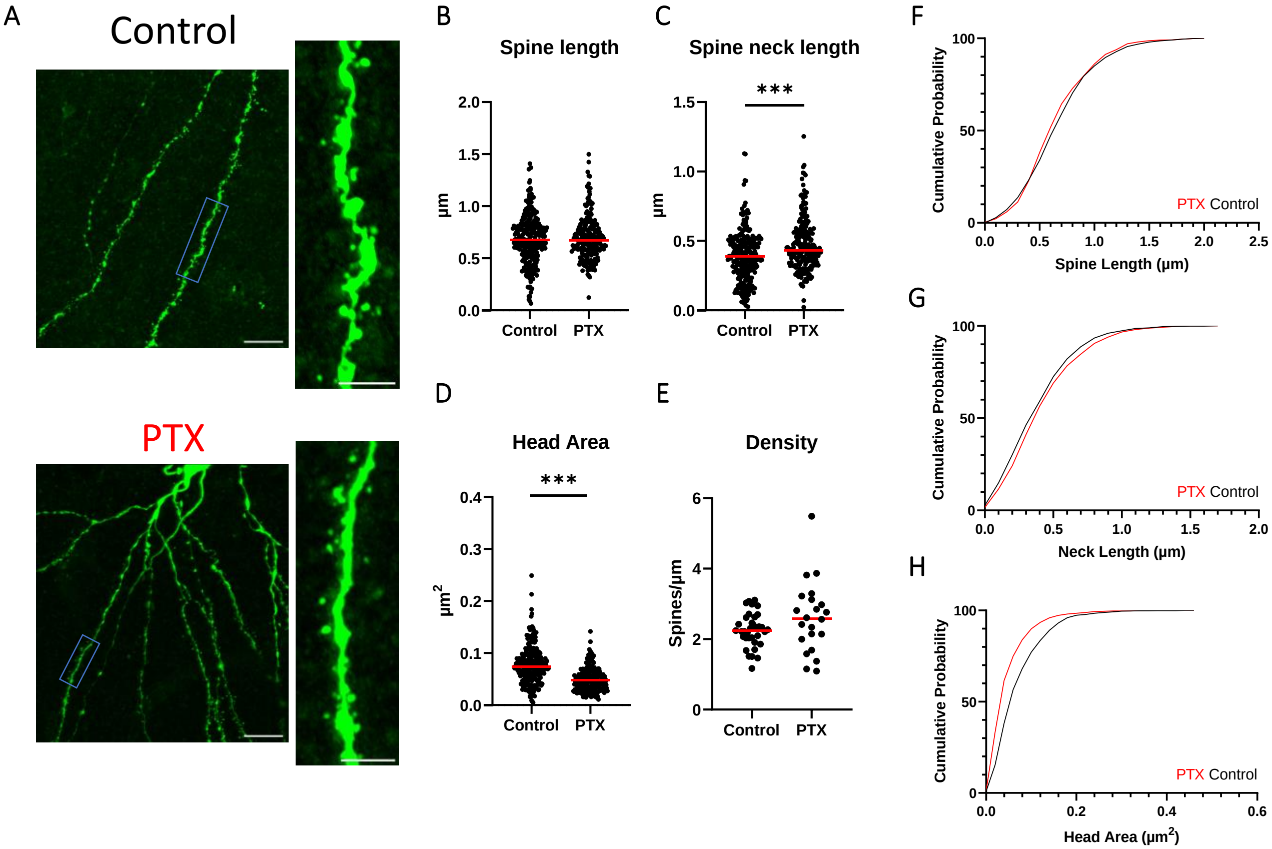

Figure 13 | Spine analysis in basal dendrites. (A) Representative image of basal dendrites in control (above) and treated group (below). Spine measurements of **(B)** spine length, **(C)** spine neck length, **(D)** head area, and **(E)** spine density. Cumulative distribution of apparent **(F)** spine length, **(G)** spine neck length, and **(H)** head area. Analysis involved n = 598 spines in 196.075 µm dendrite from 8 neurons (8 animals) for control; n = 342 spines in 276.621 µm from 6 neurons (6 animals) for treated group. Statistical analysis was performed with Mann-Whitney-U test ** p< 0.001. Shown is median. Scale bar: 10 µm for overview and 3 µm for the zoomed part.

Synaptic signaling during hyperexcitability

As we observed morphological changes in dendritic spines, we then wondered whether mild hyperexcitation conditions would lead to functional consequences in the neuronal network. To address this question, we recorded spontaneous excitatory postsynaptic currents (sEPSCs) at -70 mV under control and hyperexcitability conditions **(Figure 14)**. sEPSC serves as a robust measure to understand the synaptic function, synaptic plasticity mechanisms, and ultimately network dynamics (Veruki et al., 2003). A previous study highlighted that an increase in frequency and amplitude would heighten the effectiveness of hippocampal synapses following the onset of epilepsy in the animal model (Epsztein et al., 2006). Our experiment also allows us to investigate whether differential synaptic activity underlies differential spontaneous firing rates.

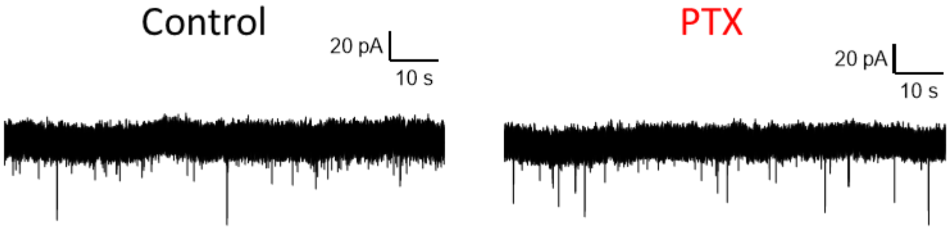

Figure 14 | GABA$_{A}$ inhibition affect presynaptic mechanism. Example traces of spontaneous EPSCs recorded at -70 mV in a CA1 pyramidal neuron in control (left) and PTX conditions (right).

We then quantified the frequency, amplitude, and other kinetic properties of the sEPSCs **(Figure 15)**. This manipulation resulted in an increased frequency occurrence (0.42 ± 0.186 Hz; p< 0.01; **Figure 15A**) and rise time 10-90% (0.0032 ± 0.0002 Hz; p< 0.01; **Figure 15E**) compared to control experiments (0.26 ± 0.015 Hz) and (0.0026 ± 0.0001 Hz), respectively. However, the enhanced neuronal activity did not affect the amplitude, half-width, decay time 90-10%, or area, hinting at a relatively stable synaptic strength. These results indicate that, again, the PTX-induced disinhibition of GABAergic synaptic transmission leads to increased excitatory synaptic activity. Specifically, this mild hyperexcitation condition primarily affects presynaptic mechanisms, which could include increased neurotransmitter release and altered synaptic transmission dynamics, rather than the postsynaptic receptor function.

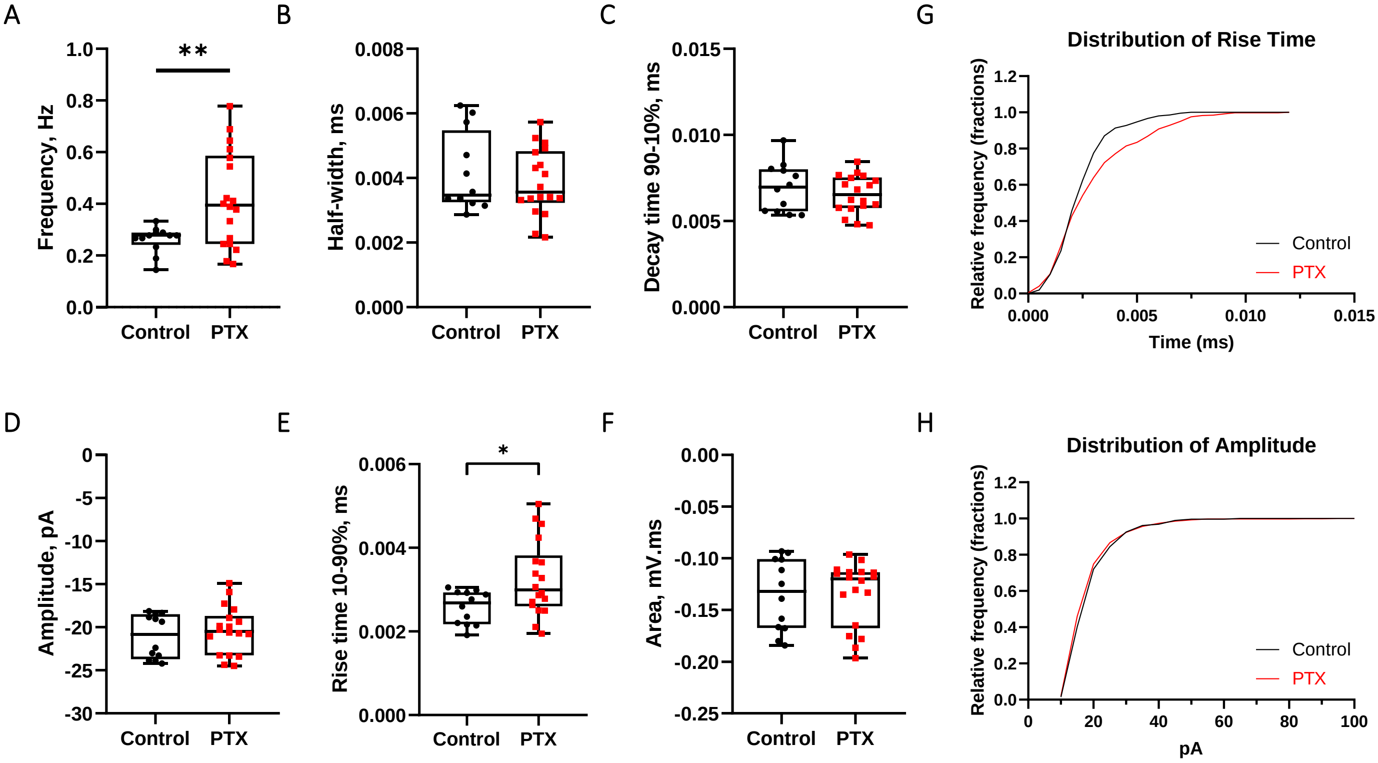

Figure 15 | Neuronal overactivation enhances synaptic inputs onto CA1 pyramidal neurons. Spontaneous excitatory postsynaptic currents (EPSCs) were recorded at -70 mV after 30 minutes of PTX application. Quantification of PTX-induced changes in **(A)** frequency, **(B)** half-width, **(C)** decay time 90-10%, **(D)** amplitude, **(E)** 10-90% rise time, and **(F)** area. Histograms of cumulative distribution in **(G)** rise-time and **(H)** amplitude. n = 10 in control and n = 10 in treated group were analyzed. Statistical analysis was performed with an unpaired T-test. * p<0.05 ** p< 0.001.

Spatiotemporal analysis of spine morphological adaptation

To follow dendritic spine adaptation over time in response to the aberrant excitatory neuronal activity, we used two-photon time-lapse imaging in acute live tissue. This sensitive technique allowed us to estimate the precise timing of changes in spine dimensions accurately. For this experiment, we used Thy1-positive animals expressing yellow fluorescent protein (YFP) in CA1 pyramidal neurons. We tracked CA1 spines across 6 sessions at 7-minute intervals **(Figure 16)**.

To induce hyperexcitability condition, we applied the $GABA_A$ blocker PTX at the beginning of the experiment and maintained its application throughout the entire 35-minute imaging session. We imaged dendritic spines in the same region of interest over time, focusing on basal dendrite, secondary apical dendrite, and tertiary apical dendrites. For spine analysis, we used SpineJ to evaluate the morphological parameters of the spines.

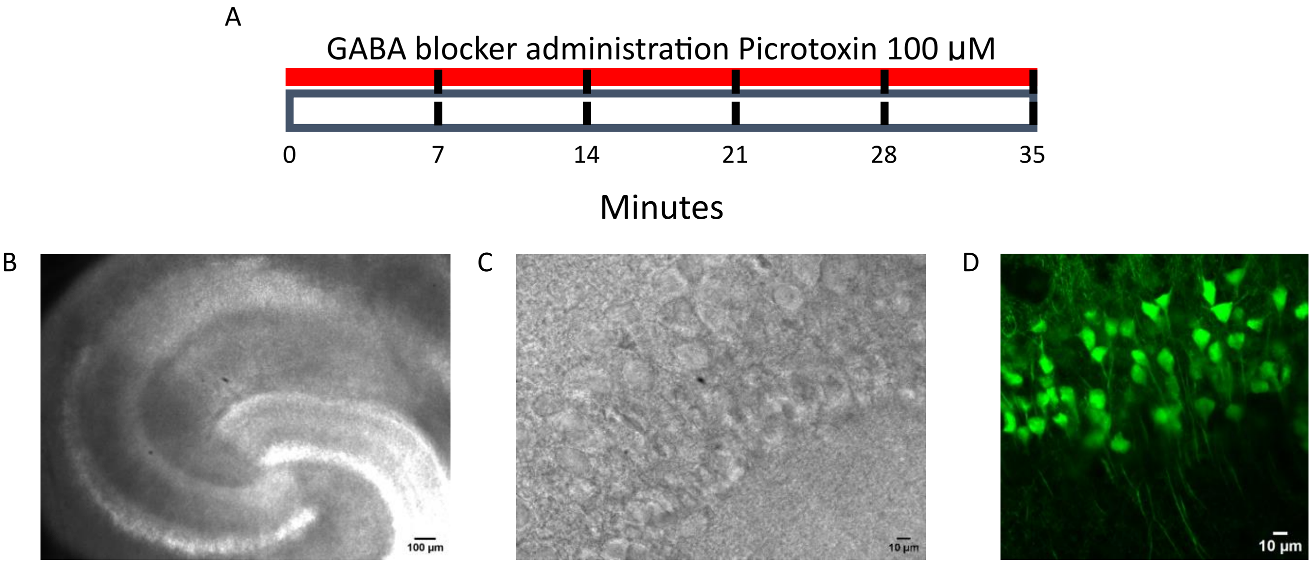

Figure 16 | YFP expression in CA1 pyramidal cells. (A) Schematic describing the time-lapse experimental timeline with 7-minutes intervals. PTX was administered continuously throughout the 35-minute experiment. **(B-C)** Light microscopy images of live acute slices **(B)** Overview of the hippocampal slice at 4x magnification**. (C)** CA1 pyramidal neurons at 20x magnification. **(D)** Two-photon image of CA1 pyramidal neurons. Cell morphology indicates that eYFP expression is limited to neurons. Scale bar: 100 µm for overview in B and 10 µm for the zoomed part in C and D.

In the secondary apical dendrite, we observed that the spines remained relatively stable during the time-lapse experiment in both the control (n = 91 spines) and treated groups (n= 56 spines; **Figure 17)**. In the control experiment, most dendritic spines maintained their initial sizes throughout the observation period, although a subset exhibited dynamic changes, including shortening, downsizing, or enlargement **(Figure 17B-D)**. However, since only a small fraction of the spine changed, the density of transient spines remained low **(Figure 17E)**. This was later confirmed by Sidak's multiple comparison test. Furthermore, the distributions of morphological parameters were similar at the beginning and end of the experiment **(Figure 17F-H)**.

In contrast, the dynamic nature of synaptic structure after PTX application showed a modest reduction based on spine length and spine neck, but not head area **(Figure 17J-M)**. Accordingly, the distribution of these parameters slightly shifted to the left **(Figure 17N-P)**.

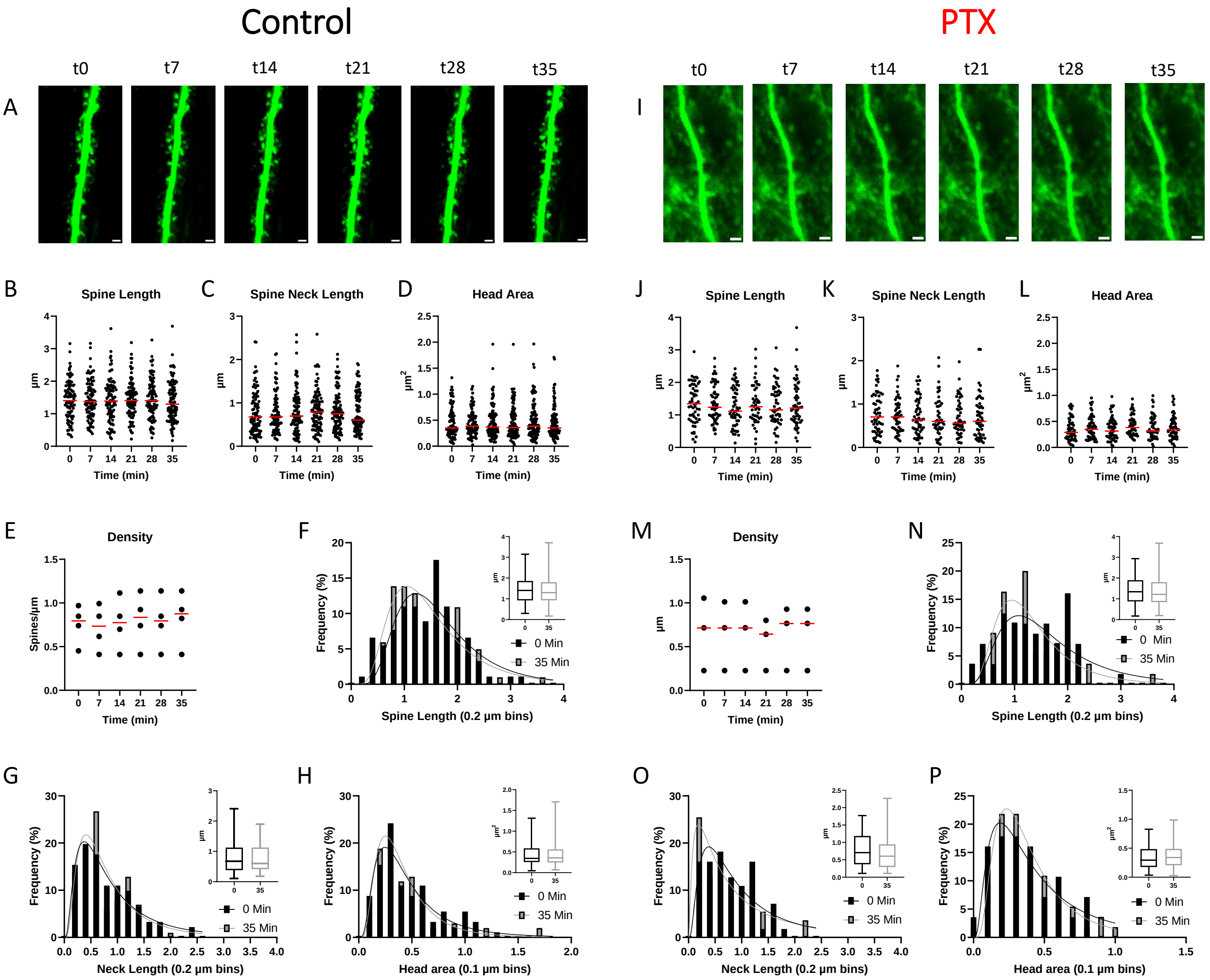

Figure 17 | Spine analysis on secondary apical dendrite. Time-lapse imaging of acute dendritic spines in control **(A)** or during PTX application **(I)** at 0, 7, 14, 21, 28, and 35 minutes. **(B-E)** Output of the spine measurement over time, including **(B)** spine length, **(C)** spine neck length, **(D)** head area, and **(E)** Density. **(F-H)** Frequency distribution of morphological parameters of spines at 0 minutes and 35 minutes. Curved lines represent log-normal fits. **(F)** Distribution of spine length measurement. **(G)** Distribution of spine neck length. **(H)** Distribution of head area. Insets show median, interquartile, and range. **(J-M)** Same as **(B-E)** and **(N-P)** same as **(F-H)** except in hyperexcitability conditions. Kruskal-Wallis analysis with Dunn's post hoc test was performed. All scale bar represent 2 µm.

Using mixed-model statistical analysis, we compared the set of experiments conducted in control and treated conditions of secondary apical dendrite **(Figure 18)**. Subsequently, we observed a statistically significant effect of PTX on spine morphology, including spine length (p = 0.0322), spine neck length (p = 0.0334), and head area (p = 0.0055; **Figure 18A-C)**. Consistent with previous experiments using fixed-tissue in the secondary apical dendrite, we found minimal changes in dendritic spine number **(Figure 18D)**. These findings suggest that the effects of picrotoxin on dendritic spines observed in this imaging study are attributable to excessive synaptic activity.

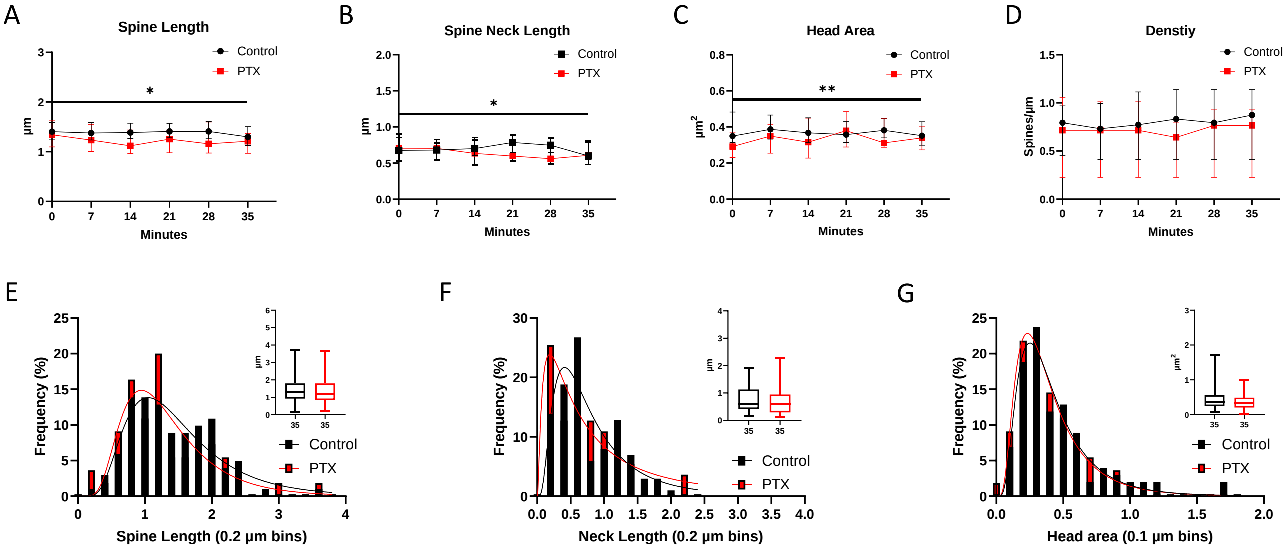

Figure 18. | Direct comparison of spine analysis on secondary apical dendrite in control versus hyperexcitable conditions. (A-D) Comparison of spine analysis over time: **(A)** Spine length. **(B)** Spine neck length. **(C)** Head Area. **(D)** Density. **(E-G)** Frequency distribution of morphological parameters at 35 minutes in control (black) and PTX (red). Curved lines are log-normal fits. **(E)** Spine length. **(F)** Spine neck length. **(G)** Head area. Insets show median, interquartile, and range. Shown in **(A-D)** is the median ± 95 CI. Statistical analysis for spine parameters was performed with a Mixed-effects model. Other comparisons were done by the Mann-Whitney U test. * p<0.05; **<0.01

We further explored spine dynamics in tertiary apical dendrites (n = 55 in control vs n = 62 in PTX group) and found that PTX had minimal effects on spine morphology and spine density **(Figure 19)**. Sidak's multiple comparison test and frequency distribution histograms indicated that changes in spine morphology were slightly smaller or shorter over the same period, though these changes were not significant. To determine whether these differences were drug-dependent, we used mixed-model statistical tests. We observed a significant effect of GABAergic disinhibition on spine length (p = 0.0174) and spine neck length (p = 0.0263), but not on head area or spine density **(Figure 20)**.

In a set of experiments on the basal dendrite, 51 spines in both the control and treated groups were imaged repetitively. Changes in spine morphology and density were monitored through z-stack image analysis. Measurement of spine length, spine neck length, head area, and density showed no specific alterations in either the control or PTX group **(Figure 21)**. These data indicate that changes detected over time were minimal in all aspects, showing a trend similar to the results observed in the apical dendrite.

Next, we compared spine adaptation over time in the control and PTX groups. Statistical analysis of this dataset showed significant differences in spine shape proportions, including spine length ($p < <0.001$), spine neck length ($p < <0.001$), and head area ($p < <0.001$; **Figure 22)**. Meanwhile, spine density remained stable without changes. Intriguingly, a very similar trend to the apical dendrite analysis was also observed, even though the proportions of spines in the control and treated groups, including spine length, spine neck length, and head area, varied greatly.

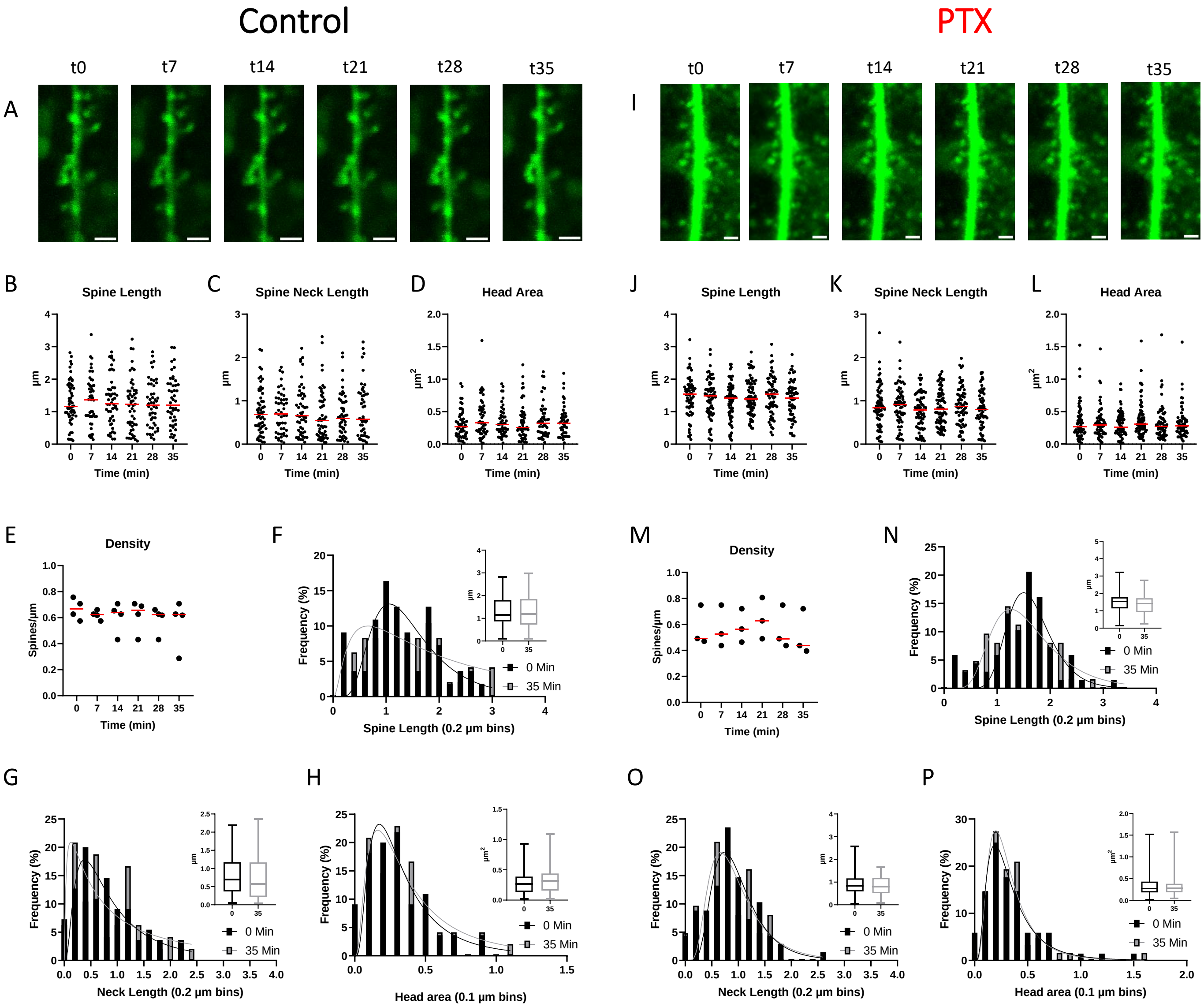

Figure 19. | Spine analysis on tertiary apical dendrites. Series of CA1 dendritic spine obtained through repetitive 2-photon imaging of the same segment with 7 minutes interval in **(A)** control and **(I)** in treated conditions. **(B-E)** Scatter plot showing the dynamic changes in spine morphology: **(B)** Spine length, **(C)** Spine neck length, **(D)** Head area, and **(E)** density detected over time. **(F-H)** Distribution of changes in spine morphology at 0 (black) and 35 minutes (grey). Curved lines are log-normal fits. Insets show median, interquartile, and range. **(J-M)** Same as **(B-E)** and **(N-P)** same as **(F-H)** except in hyperexcitability conditions. Kruskal-Wallis analysis with Dunn's post hoc test was performed. All scale bar represents 2 μm

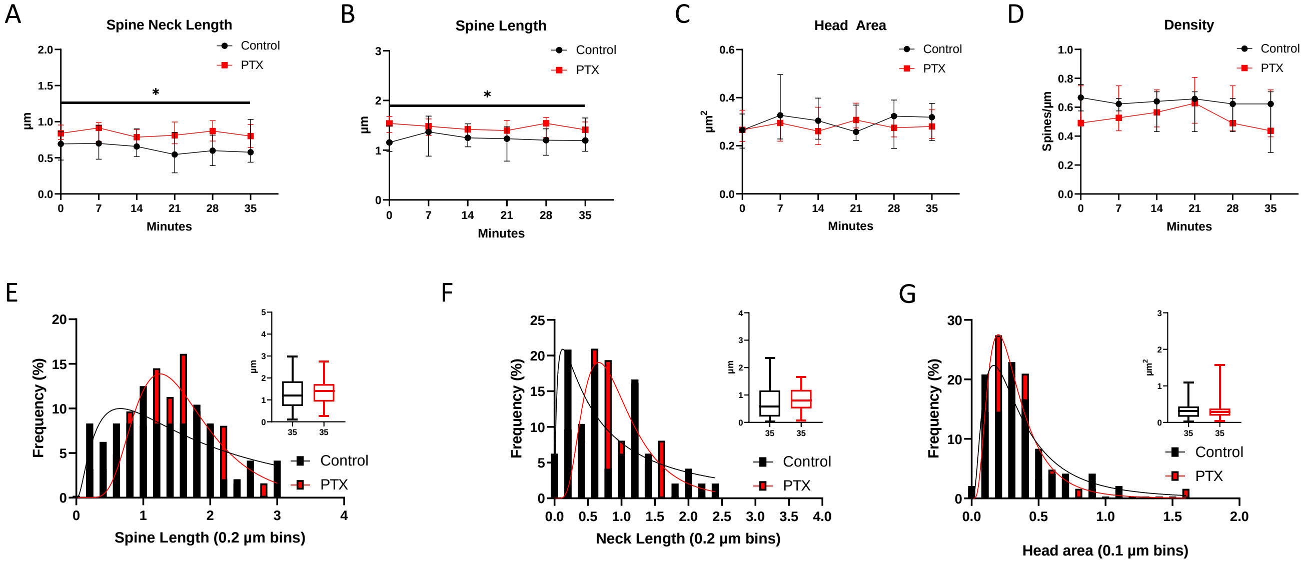

Figure 20. | Changes in the spine morphology of tertiary apical dendrites induced by PTX application. (A-D) Comparison of spine morphology changes measured over time in control (black) versus hyperexcitable condition (red): **(A)** Spine neck length, **(B)** spine length, **(C)** head area, and **(D)** density. **(E-G)** Histograms display the distribution of spine structures in the control (black) and treated group (red) at minute 35: **(E)** Spine length. **(F)** Spine neck length. **(G)** Head area. Insets show median, interquartile, and range. Shown in **(A-D)** is the median ± 95 CI. Statistical analysis for spine parameters was performed using a Mixed-effects model. Other comparisons were done by the Mann-Whitney U test. * $p<0.05$

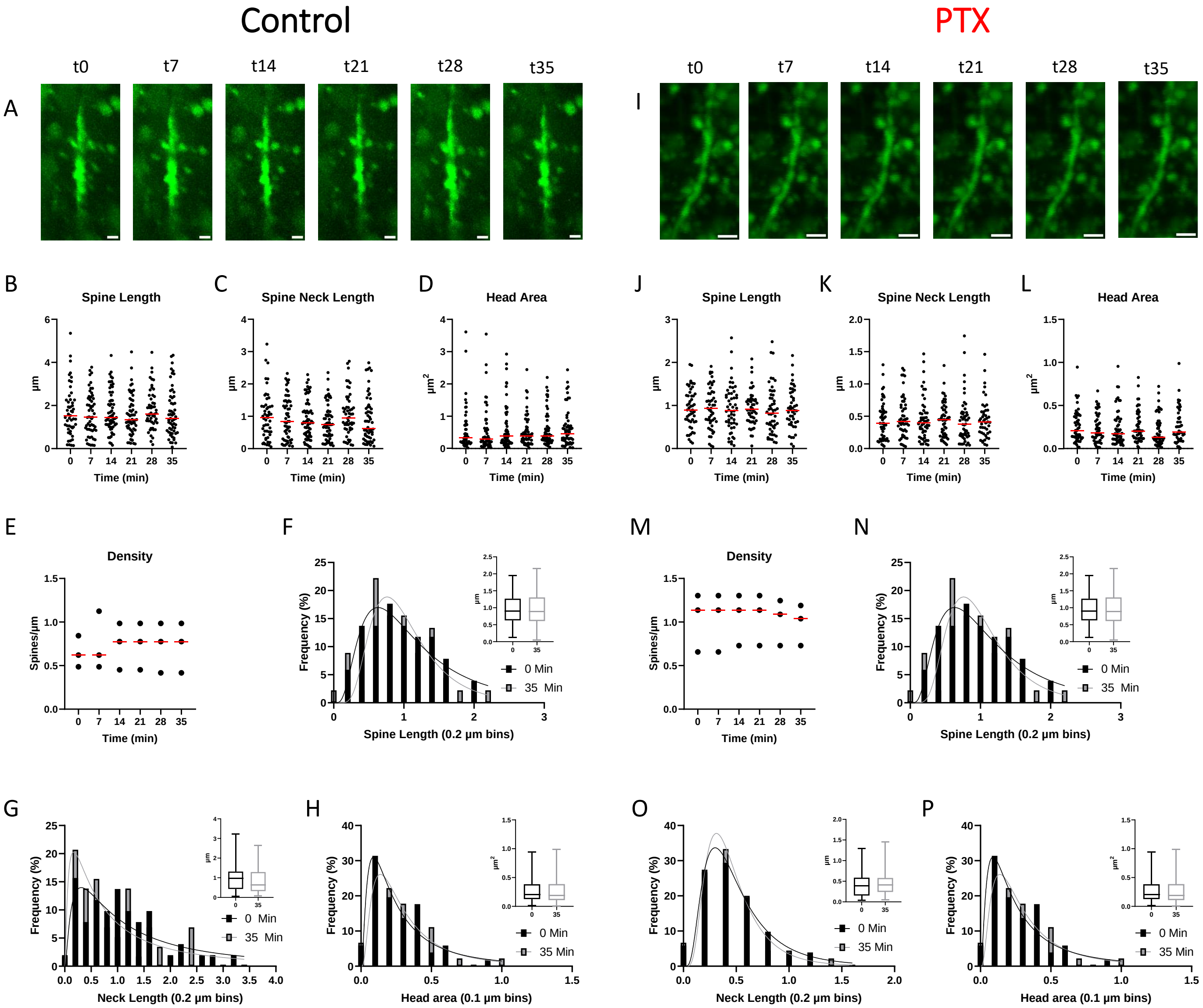

Figure 21. | Spine analysis on basal dendrites. Illustration of a dendritic segment expressing Thy1 in control **(A)** or during PTX application **(I),** at different time points. **(B-E)** Quantitative morphological analysis of visible spines over time, showing **(B)** spine length, **(C)** spine neck length, **(D)** head area, and **(E)** Density. **(F-H)** Distribution of spine morphology at 0 and 35 Minutes: **(F)** Distribution of apparent spine length, **(G)** spine neck length, **(H)** head area. Curved lines represent log-normal fits. Insets show median, interquartile, and range. **(J-M)** Same as **(B-E)** and **(N-P)** same as **(F-H)** except in hyperexcitability conditions. Kruskal-Wallis analysis with Dunn's post hoc test was performed. All scale bar represents 2 µm.

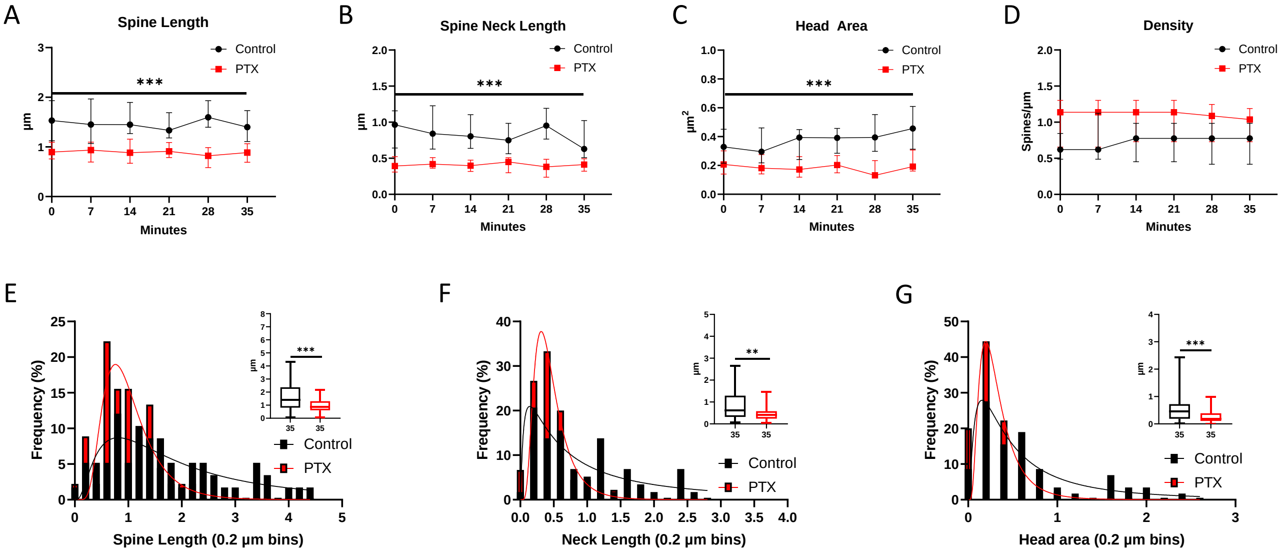

Figure 22. | Spine adaptation in basal dendrites following PTX administration. (A-D) Comparison of spine morphology and density in control (black) and hyperexcitation condition (red)**.** Image-J reported the spine analysis for **(A)** spine length, **(B)** spine neck length, **(C)** head area, and **(D)** density. Shown is the median ± 95 confidence interval (CI). Statistical analysis was performed using a Mixed-effects model. **(E-G)** Distribution of spine structures in control (black) and treated group (red) at 35 minutes: **(E)** spine length, **(F)** spine neck length, and **(G)** head area. Insets show median, interquartile, and range. Statistical analysis was performed using Mann-Whitney U test. *** p<0.001

Discussion

By analyzing neuronal behavior and dendritic spine morphology in the early stages of increased neuronal activity, we provide new insights into the mechanisms underlying neuronal adaptation in CA1 pyramidal neurons. Picrotoxin-induced hyperactivity conditions in our acute hippocampal slices served as a reliable experimental model. Several meaningful interpretations, contextualization, and implications of our experiments are summarized below.

Selecting GABAergic mechanism in CA1 pyramidal neurons as the primary manipulator

Oversimplified frameworks of epilepsy propose imbalances between excitatory and inhibitory signals. Disruptions in either excitatory or inhibitory mechanisms within neuronal networks are believed to induce hyperactivity and synchronization of neuronal firing (Becker, 2018). To mimic this condition in our experimental model, we opted to work with either excitatory or inhibitory mechanisms. In our defense, we argue that modifying the activity of neurons and then later measuring the resulting changes in those neurons can undermine the legitimacy of the results. In this sense, analyzing KA-induced epileptiform activity, primarily driven by excitatory mechanisms, is challenging because it is difficult to attribute the observed effects solely to the activation of kainic acid receptors. Moreover, KA, an analog of glutamate, induces excitotoxicity, resulting in neuronal damage and cell death (Cavazos & Cross, 2006; Ueda et al., 2002). Therefore, selective inhibition of inhibitory synapses would facilitate a precise examination of excitatory synaptic transmission without any confounding influence of inhibitory signals.

Using PTX as the experimental model

Our initial experiment confirmed that picrotoxin (PTX), a $GABA_A$ inhibitor, can induce hyperactivity. This is evidenced by the increased number of frequencies observed in field potential and cell-attached recordings. The disinhibition of GABAergic function indeed suggests an active participation of GABAergic neurons in controlling cellular behavior. Spatially, CA1 pyramidal neurons are surrounded by at least 21 classes of interneurons and predominantly receive GABAergic input on their dendrites (Kanemoto et al., 2011; Klausberger & Somogyi, 2008) At this point, various factors could potentially contribute to these observed results. The increased firing frequency resulting from the PTX application aligns with findings from other experimental epilepsy models, where similar heightened neuronal activity was observed using similar or different drugs. This signifies a shift in the balance of excitation/inhibition within the neuronal network (Becker, 2018; Cavazos & Cross, 2006; Ergina et al., 2021; Martín-Suárez et al., 2023).

Evaluating intrinsic properties for insights into the functional dynamics of a neuron

Neuronal intrinsic properties appear to be crucial for maintaining the neuron’s readiness to generate action potential (Beck & Yaari, 2008). In our study, we observed no major changes in the intrinsic properties or excitability features of the CA1 hippocampal region. However, we did observe an increased number of APs fired at the potential threshold, which can be attributed to the increased neuronal input. While the disinhibition mechanism induced by PTX directly heightened neuronal activity, it did not play a significant role in regulating intrinsic properties and neuronal excitability. A similar study using 4-aminopyridine (4-AP), to induce hyperexcitability via glutamate release and overactivation of glutamate receptors, also found no significant difference in essential biophysical properties (Ergina et al., 2021). However, some findings are somewhat contradictory due to differences in the experimental model. For example, studies on Dravet syndrome using iPSC lines and mouse models have shown significant changes in intrinsic properties following the onset of seizures (Almog et al., 2022; Dyment et al., 2020; Jones et al., 2022). At least, we can speculate on the importance of intrinsic properties in maintaining cellular resilience. Taken together, it appears that the neurons in our study model maintain homeostatic conditions despite increased firing rates and altered network activity.

Neuronal hyperactivation induces spine morphological rearrangements

Previous data indicated that disruption of inhibitory neurotransmission could have a robust effect on the overall network activity. This potentiation of excitatory synapses can effectively alter spine morphology, all of which modulate and accommodate signal transmission between neurons (Pchitskaya & Bezprozvanny, 2020). Our current results confirm and extend our knowledge of spine rearrangements induced by synaptic disinhibition through PTX application.

In apical dendrite, we observed massive spine remodeling in secondary but not tertiary apical dendrite. Shorter spine length, reduced spine neck length, and smaller head area could therefore reflect a compensatory mechanism. A smaller head area typically indicates a reduced postsynaptic density (Arellano et al., 2007). This proportional adjustment also coincides with the number of receptors and synaptic strength (Anggono & Huganir, 2012). Therefore, spatially confined inhibition to limit the synaptic input was prominently observed. Consistently, it has also been reported that the proximal segment of the apical dendrite receives more input from GABAergic interneurons than its distal part (Papp et al., 2001). Hence, the disinhibition of GABAergic neurons in the proximal segment, especially in secondary apical dendrite, may also explain the larger picrotoxin effect in spine remodeling.

Growing evidence highlights the significance of the spine neck in regulating signal transduction efficiency, with shorter spine necks indicating higher effectiveness (Tønnesen et al., 2014). To understand how the spine neck can fine-tune the synaptic input, cable theory can be applied to dendritic spines to explain how electrical signals propagate. According to cable theory, the electrical properties of the spine neck, such as its length and diameter, contribute to its resistance. Therefore, this plastic ability of the spine neck to resize could act as a resistor, influencing the electrical signals that pass through it.

A computational study in a younger individual also showed a cluster of small spines believed to be crucial for the learning process and synaptic plasticity (Pchitskaya & Bezprozvanny, 2020). We could then speculate that neurons are preparing for a selective process to modulate signal efficacy. In other words, neurons in the secondary apical dendrite might adjust their spine structure to counteract the increased excitability in the nearby region in order to maintain their homeostatic intrinsic properties.

Spines on basal dendrite, on the other hand, displayed longer neck lengths combined with smaller head areas. We argue that this is mainly due to noticeable differences in the inputs to the basal and apical branches. Basal dendrites receive more input from CA3 neurons and Schaffer collaterals (Spruston, 2008). In terms of GABAergic input, a distinct distribution of a subset of GABAergic interneurons can also be observed (Klausberger & Somogyi, 2008). These structural and input variations highlight the functional specialization of basal dendrites in neuronal processing.

A thin, longer spine neck has a high electrical resistance, limiting the amount of current that can flow from the spine head to the dendrite. As a result, this high resistance can isolate the spine head electrically, attenuate the synaptic strength, and ensure the signal received is not easily spread to the dendrite. Furthermore, a smaller spine head indicates a lower capacitance, which means it can store less electrical charge. With a smaller spine head area in the basal dendrite, the proportion of signal attenuation due to the neck's resistance increases. Altogether, this spine rearrangement helps to ensure that synaptic inputs are precisely regulated.

It has also been proposed that thinner spines are more unstable and contribute to weak or silent synaptic connections (von Bohlen und Halbach, 2009). This instability could then be a mechanism for synaptic pruning or a form of synaptic plasticity. These spine characteristics in basal dendrites hint at a regulation of the magnitude of post-synaptic potential, indicating that various inputs and locations result in distinct morphological arrangements.

Interestingly, our dataset collectively showed a stable number of spines across the dendrites. We speculate that a delicate alteration in spine structure as an immediate response is favorable rather than eliminating the existing synapse or forming a new synapse. Although no information is available on spine number organization following an epileptiform activity, the earliest measured effect of Gabazine, a competitive antagonist of $GABA_A$ receptors, showed a 50% reduction in spine density after 48 hours (Zha et al., 2005). Hence, balancing spine morphology, elimination, and plasticity is crucial for optimal brain function.

Complex effects of PTX-mediated hyperexcitability in synaptic communication

We examined the functional properties of spontaneous EPSCs. Our analysis of the parameters of spontaneous EPSCs revealed different responses after 30 minutes of PTX application. We observed an increase in frequency and rise time but not in amplitude and other kinetic parameters. To interpret this neuronal reaction, it is necessary to understand what the results might indicate.

Firstly, increased frequency could suggest a heightened excitatory input onto the postsynaptic neuron. This could imply an increase in vesicle release probability, presynaptic activity, or changes in synaptic connectivity (Cavazos & Cross, 2006; Clarkson et al., 2020; Shim et al., 2018). To our surprise, we found no evidence of an enhanced amplitude or amplitude reduction but rather a stable amplitude. A similar result was also reported in a study of KA-induced status epilepticus (Clarkson et al., 2020). The amplitude of the sEPSC is believed to be mainly modulated by the number and sensitivity of postsynaptic receptors (Liao et al., 1995). Thus, one could argue that the GABAergic disinhibition primarily influences network excitability without altering postsynaptic efficacy in neurotransmission.

Secondly, in terms of kinetic properties of the neurons, we only observed a longer rise time, which reflects a slower rate of postsynaptic current onset and probably, a temporal summation of AP generation. We found no significant change in half-width and decay time. Alternatively, adjustments in neuronal behavior could potentially occur. For example, changes in postsynaptic receptor properties (Veruki et al., 2003). In the present study, increased frequency in the presynaptic may induce receptor desensitization after several minutes. This compensatory mechanism is believed to be used against the bombardment of network hyperexcitability. We could also further speculate that this adaptation did not change the ratio of AMPA/NMDA receptor as seen in the amplitude, decay, and half—width parameter (Rakhade et al., 2008; Veruki et al., 2003).

Overall, we might observe a delicate interplay between presynaptic and postsynaptic factors in controlling the hyperexcitability condition induced by PTX. Even though the underlying mechanism is not immediately obvious, these findings corroborate our electrophysiological data and structural study.

Unveiling electrophysiological insights and spine morphological alterations

Despite the evidence showing a direct correlation and causation in every experiment, it is necessary to explain our findings on a broader scope. By combining these electrophysiological results with our fixed-tissue studies on spine morphology, we notice a biological significance in neuronal adaptations, which are relevant to the process of increased network excitability. Specifically, selective disinhibition of CA1 pyramidal neurons effectively increased network activity, followed by spine reorganization. Notably, smaller head areas and shorter spines, as seen in apical dendrites, seem to retract and avoid the hyperactive neurons. Spine shrinkage also appears to limit synaptic contact and is likely to increase neck resistance. A slower rise time could hint at a crucial role in controlling the timing of AP generation, which reflects ongoing plasticity. In this situation, highly synchronized signals at some point would be likely to appear. Additionally, manipulating the activity of CA1 neurons could also trigger receptor desensitization. Importantly, none of the other kinetics in sEPSCs showed any significant alterations, as well as the intrinsic and neuroexcitability properties. This is useful to consider because there are no other adjustments rather than morphological adaptations (Rakhade et al., 2008; Veruki et al., 2003). Therefore, spine morphology adjustment appears to have a rapid protective effect during mild hyperexcitation conditions.

Exploring spine dynamics during PTX application

Dynamic change and long-term stabilization of dendritic spines are highly associated with neuronal activity (Holtmaat et al., 2006; Hotulainen & Hoogenraad, 2010). Changes in spine density as well as impairments in spine structure, have been reported in several experimental models of epilepsy and numerous neurological disorders (Fiala et al., 2002; Penzes et al., 2011; Wong & Guo, 2013). As a crucial site for excitatory synapse, spines can interfere with synaptic strength and functional connectivity (Tønnesen et al., 2014). It is thus natural to closely investigate the evolution of spine dynamics in response to PTX.

In line with our observations in fixed tissue, our time-lapse live imaging showed an overall effect of PTX in dendritic spine dynamics over time. Yet, there were no measurable differences within each group, suggesting that they displayed a relatively stable spine structure for 35 minutes. Similar work also reported persistent structural stability of spines after 30 minutes of exposure to epileptic seizures (Mizrahi et al., 2004). In this study, Mizrahi et al. used bicuculine, a competitive antagonist of the $GABA_A$ receptor, and a single dose of pilocarpine, a muscarinic acetylcholine receptor agonist, to induce seizures. Taken together, our experiment confirms the minimal spine dynamics and may reflect the importance of spine distribution in maintaining the normal physiology of neuron complexes, especially during hyperexcitability conditions.

In principle, it is challenging to use two-photon microscopy as an imaging modality to visualize nanoscale structures, including dendritic spines, axonal shafts, and boutons. The lack of spatial resolution hinders the detailed visualization of dendritic spines (Arellano et al., 2007; Calovi et al., 2021; Levet et al., 2020). Typically, longer light wavelength results in a wider point-spread function (PSF), which exceeds 350 nm in two-photon microscopy (Tønnesen & Nägerl, 2013), making it difficult to precisely estimate fine structural details as well as subtle changes in the experimental model.

Given the importance of this spatial resolution, we noticed result differences in spine density obtained from fixed-tissue and live imaging, which are approximately 3 spines/µm and 1 spines/µm, respectively. This proportional difference was also observed when comparing results from two-photon and electron microscopy (Attardo et al., 2015; Gu et al., 2014; Harris et al., 1992; Mizrahi et al., 2004). Furthermore, it remains difficult to adequately resolve spine neck length as they are typically in a median of 551 nm observed in acute slices and 667 nm observed in organotypic culture (Tønnesen et al., 2014). This reported value is much closer to our fixed-tissue study with a lesser extent to our two-photon measurement. Despite of this low resolution, two photon microscopy offers a deep tissue penetration as much as 700 µm and reduced phototoxicity as its main advantages (Mizrahi et al., 2004).

Future Direction

Although current efforts to explain the functional and structural changes in dendritic spines following neuronal hyperactivation have greatly expanded our understanding, we propose several experiments that could serve as very promising future directions to focus on:

Re-evaluation of findings using STED microscopy

The present study highlighted the crucial role of dendritic spines in regulating synaptic transmission, revealing significant insights into spine remodeling in the absence of synaptic plasticity. To corroborate the observed results, the use of Stimulated Emission Depletion (STED) microscopy would be very useful. STED offers super-resolution imaging capabilities that exceed the diffraction limit of confocal microscopy, enabling the visualization of dendritic spines with higher precision. We speculate that this advanced imaging technique will allow for a more detailed examination of the structural changes in dendritic spines, potentially revealing finer aspects of spine necks that were previously undetectable.

Astrocytic coverage during mild hyperexcitation condition

Besides the dendritic spine, it is also interesting to investigate the role of astrocytes in the early stage of increased network excitability. Astrocytes play a crucial role in controlling extracellular glutamate concentration, specifically, through rapid glutamate clearance following synaptic transmission in the synaptic cleft (Verkhratsky & Nedergaard, 2014). It is thus interesting to explore the astrocytic coverage of spines in this experimental model, which could potentially compensate for and fill any synaptic gaps resulting from spine retraction, as proposed in this thesis.

Extracellular space

In a complex disease like epilepsy, disease progression may be influenced by several key players. During the disease development, it would be interesting to gain dynamic insights into how changes in extracellular space (ECS) occur and establish a temporal relationship in response to increased neuronal activity. Additionally, our lab has established and pioneered a novel imaging technique called super-resolution shadow imaging (SUSHI) to assess extracellular space (ECS) microstructure (Tønnesen et al., 2018).

Conclusions

In this thesis, we explored various approaches aimed at understanding the earliest functional and morphological adaptations to hyperexcitability in the hippocampal circuit. Using picrotoxin (PTX), a non-competitive antagonist of $GABA_A$ receptors, we induced modest hyperexcitation in mouse hippocampal acute slices. Specifically, we revealed the neuronal excitability properties and the involvement of dendritic spines, most of which are key mechanisms underlying increased network excitability, in the context of shaping overall output amidst neuronal hyperactivity.

Firstly, our experimental model of hyperexcitability provided valuable insights into the increased network activity and enabled us to dissect the dynamic changes occurring at the neuronal, synaptic, and network levels.

Secondly, electrophysiological results from whole-cell recordings exhibited unaltered intrinsic excitability properties, demonstrating a mechanism of homeostasis. Consistently, disinhibition of CA1 pyramidal neurons significantly enhanced synaptic strength and spine accommodation.

Thirdly, confocal imaging of fixed-tissue studies revealed structural changes in dendritic spines. We demonstrated that spines function as a “structural-functional” manager at CA1 pyramidal neurons during mild hyperexcitation conditions, precisely controlling hyperactivity input via their smaller head area.

Fourthly, we described the effect of PTX in spontaneous EPSCs, showing increased frequency and longer rise time without affecting amplitude, half-width, and decay time.

Fifthly, the timelapse of live-cell imaging showed stable spine density after a brief period of hyperexcitability.

In conclusion, the research presented in this thesis highlights the crucial adaptations of dendritic spines in maintaining normal function and how they may be influenced by modest hyperexcitable conditions.

Collaborations

Functional assessment of olfactory neuroepithelium cells in bipolar disorder patient

This work is a collaborative project with Alejandra Delgado Sequera and Esther Berrocoso from Cadiz University (Universidad de Cadiz) from May – July 2021

Introduction

Cannabis is the third most abused psychoactive substance and is also being explored as a potential therapeutic drug, necessitating a comprehensive understanding of its effects on the human brain. Previously, the group of Berrocoso used olfactory neuroepithelium (ONE), a peripheral nervous tissue that shares similar features with the central nervous system, to investigate the substantial alterations in protein expression between chronic cannabis users and healthy control (Delgado-Sequera et al., 2021).

Inspired by this study, Alejandra aimed to examine the protein expression levels and neuronal behavior in patients with bipolar disorder (BD) backgrounds. In this collaborative study, we addressed the latter issue by exploring basic neuronal electrical activity, including intrinsic electrical properties and neuronal firing patterns. Furthermore, we also monitored cell development in cultured cells to provide valuable insights into age-related changes in growth and differentiation.

Our results showed that ONE cells in a BD background have a resting membrane potential (RMP) of -16.86 ± 3.367 mV from 10 days in vitro (DIV) to 31 DIV. Moreover, no action potentials were observed during the recording. This aberrant RMP could indicate issues in ion channel dysfunction or other factors affecting membrane permeability, hinting at a problem in the maturation process. By examining these possible mechanisms, we can gain a deeper understanding of BD.

Materials and Methods

Cell Cultures

The olfactory Neuroepithelium Cells (ON) were cultured in a 1:1 medio-mix of EBM^{TM}-2 (LONZA) and Neurobasal medium (Thermo Fisher Scientific), supplemented with 5% fetal bovine serum (FBS) (GIBCO), 1% Antibiotic-Antimycotic (Biowest), 2% of B27, 5µM Forskolin, 1 µM retinoic acid, and 2% GlutaMAX (GIBCO). The cells were maintained in T75 or T25 Nunc EasYFlask (Thermo Scientific) and incubated in a humidified atmosphere containing 5% CO_2 and 95% air at 37°C. The medium was refreshed thrice weekly, and the cells were maintained at 80% confluence. For electrophysiological recording, cells were seeded on coverslips coated with poly-l-lysine at 80% confluence.

Electrophysiology Recordings

Coverslip covered with ONE cells were recorded at the corresponding DIV using a HEKA EPC10 double amplifier and controlled with HEKA Fitmaster Software. The recording chamber was perfused with ACSF containing (in mM) 119 NaCl, 2.5 KCl, 1.6 $MgCl_2$, 26 $NaHCO_3$, 1 NaH_2PO_4, 5 HEPES, 10 Glucose, and 2.5 $CaCl_2$ (300-310 mOsm; pH 7.4) at a rate of 2.5 mL/min. Cells were randomly selected without any prejudice. Glass electrodes (4 - 6 MΩ) were pulled from standard-wall borosilicate capillaries (Science Products Gmbh) and filled with intracellular solution composed of (in mM) K-gluconate 125, KCl 5, HEPES 10, EGTA 1, Mg-ATP 4, Na2-GTP 0.3, NaP-creatine 10 and L-ascorbic acid 3 (285-290 mOsm, 7.3 pH).

Cells were recorded using a similar protocol to that described above for intrinsic evaluation. This included a ramp injection and current step protocol. In addition to the latter, we injected a current step from -600 pA to +270 pA with increments of 30 pA in a total of 30 sweeps. This aimed to obtain extensive coverage of the cell reactions.

Data Analysis

Electrophysiology results were analyzed using FitMaster, Nest-o-Patch, and GraphPad Prism 8.0.

Results

Olfactory neuro epithelium (ONE) cell intrinsic properties

We initiated the characterization of olfactory neuro epithelium (ONE) cell development by examining its behavioral manifestation. Whole-cell recordings were used to assess neuronal electrical properties from 6 DIV to 31 DIV (**Fig. 1A**). Cultured neurons from both control and BD patients did not exhibit any response to current steps, (**Fig. 1C**) (from -100 pA to + 280 pA with an increment of 20 PA), voltage steps (**Fig. 1E**) (from -80 mV to +15 mV with an increment of 5 mV), or the current ramp protocol (from 0 pA to 500 pA in 1s) (**Fig. 1G**). Furthermore, to illustrate the differences in cell responses, we plotted the current-voltage (IV) relationships between the step protocols and the membrane potentials (**Fig. 1D**). In terms of resting membrane potential recorded at 0 pA, we observed that the RMP of ONE cells in BD patients was -16.86 ± 3.367 mV, whereas it was -54.78 ± 7.17 mV in control cells (**Fig. 1F)**. It is also worth noting that although these cells were unable to generate action potentials, their morphological development exhibited similar features to typical neurons. Taken together, these results indicate the inability of ONE cells to function as neurons by firing action potentials.

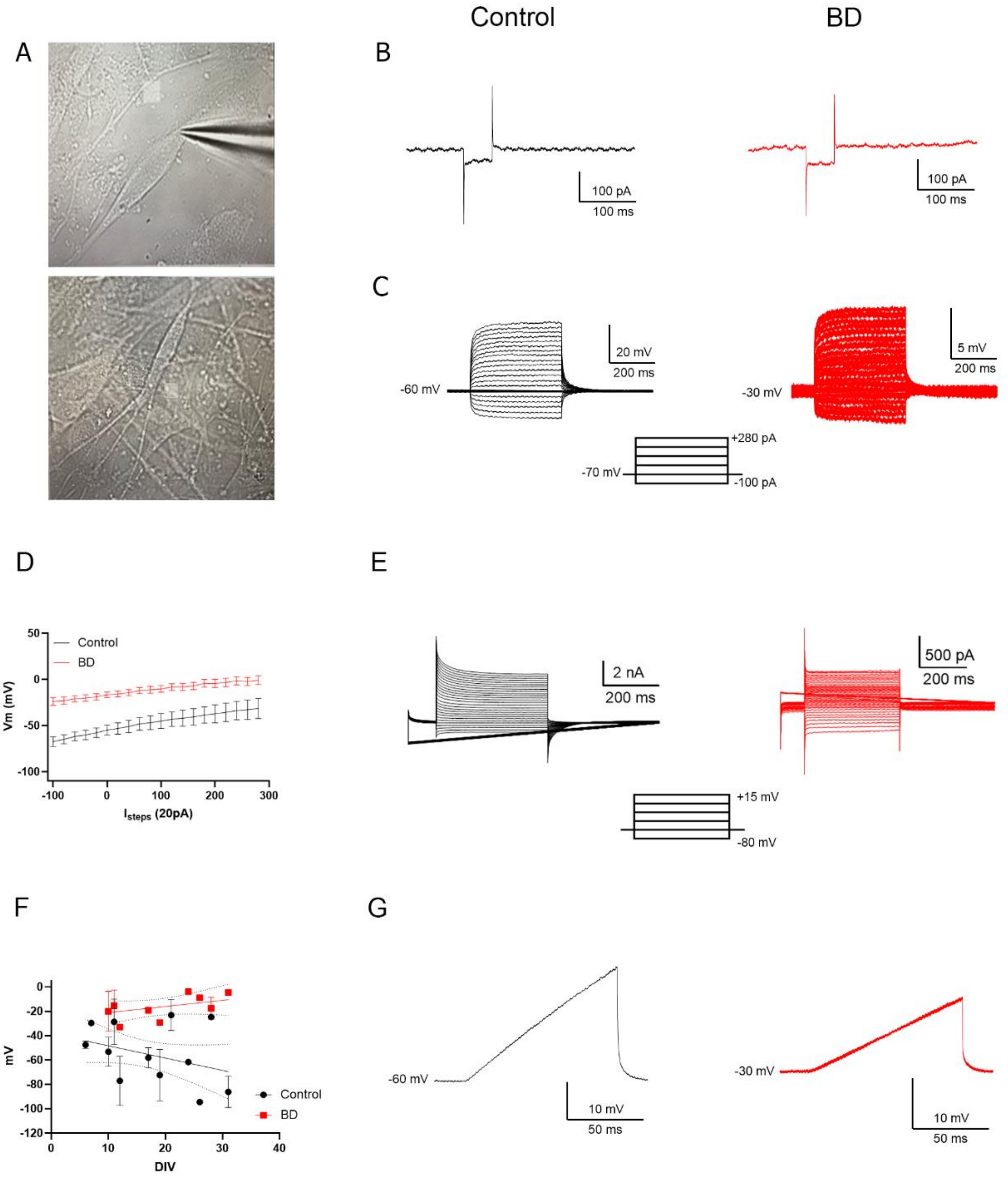

Figure 23. | ONE cell in the BD background fail to fire an action potential. Cell activity was recorded via whole-cell recording. **(A)** Example cell images from control (above) and BD background (below). **(B,C,E,G)** Representative traces from wild-type (left, black) and BD background (right, red), showing the cell responses to a test pulse of 5 mV **(B),** a current step from -100 pA to +280 pA in 20 sweeps **(C),** a voltage step from -80 mV to +15 mV in 20 sweeps **(E),** and a depolarizing ramp current injection from 0-500 pA in 1s **(G).** The cartoon below illustrates the recording protocol conditions. **(D)** Current step (Istep) IV relationship. Median ± 95 CI. **(F)** Resting membrane potential across the DIV in wild-type (black) and BD background (red). Mean ± SEM.

Discussion

The use of olfactory neuroepithelium cells in elucidating the molecular mechanisms of diseases has been widely adopted (Galindo et al., 2018; Delgado-Sequera et al., 2021). In the present study, we focused on their basic neuronal electrical properties as part of the collaboration. We found that cells from both control and BD backgrounds failed to generate an action potential. Additionally, the resting membrane potential of BD cells was significantly more depolarized compared to the control. These results strongly suggest that the cells could not progress in their neurophysiological development, ultimately affecting their ability to engage in essential cellular communication. Interestingly, our morphological assessment showed that both ONE cells from the control and BD backgrounds closely resembled neuronal cells.

This result differs somewhat from the previous study by Galindo et al, in which they reported a cellular response to 20ms steps at different voltages. We could speculate that there is a profound problem in cell maturation based on the value of the RMP. The resting membrane potential is an essential parameter for cell physiology, determined by the distribution of ions across the cell membrane. Furthermore, cells undergo various stages during development, and the RMP will be adjusted accordingly. Our study thus unveils crucial disruptions in BD in regulating membrane potentials. However, precisely how BD impairs the organization of a membrane remains to be elucidated. At least, such deviations can be a clear sign of cellular dysfunction, and hence, future experiments will need to address how BD is involved in the underlying issues during development.

Conclusion

Our study reveals that bipolar disorder disrupts basic neuronal electrical properties, impairing action potential generation and altering resting membrane potential in olfactory neuroepithelium cells. This highlights potential issues in cellular maturation and communication.

Acknowledgments

Alhamdulillah! The journey of my PhD chapter has finally come to an end. I want to take this opportunity to express my feelings and appreciation to those who played crucial roles in completing my PhD project. These remarkable five years of research were filled with both highs and lows. But the constant support, help, and love from my colleagues, friends, and family made my PhD journey more cheerful and colorful.

First and foremost, I would like to express my heartfelt gratitude to my PhD supervisor, **Dr. Jan Tønnesen**. Thank you for trusting me and allowing working with you. It is truly an honor. In those early days, my result-oriented mind was always racing for the next experiment, constantly worrying about the quality of my research output. But somehow, your constructive advice and encouragement made this journey more enjoyable and compelling. Overall, I can confidently say that I have learned and upgraded my skills in the scientific world and my daily activities.

I extend my heartfelt thanks to the members of the Neuronal Excitability Lab: **Paula, Ane, Dann, Jonny, and Virginia,** as well as the previous member, **Juan,** for their insightful comments and contributions to my work**.** It is necessary for me to honorably mention **Paula** and **Ane**. Your help, both in and out of science, has been indispensable. It has been a pleasure collaborating with you two. *Muchas Gracias!*

Special thanks to **Dr. Ricardo Andrade** for his assistance with Airyscan. Your expertise in imaging has been critical to this PhD research, and I owe you an immeasurable debt of gratitude. I am also grateful to have Dr. Cristina Miguelez Palomo on our team. Your help with animal issues has been instrumental in maintaining our experimental schedule.

I want to thank the Achucarro staff, including **Jaime, Aitor, Laura, Alejandro,** and **Izaskun**. Their commitment to improving science is beyond excellence.

My friends and family, thank you for showering me with encouragement, love, and understanding throughout this academic pursuit. **Aki, Oma, Bobi, and Moma,** your support has sustained me during the challenging and rewarding times. **Abang, Alifa, Ami, Fatimah, Kabunga, and Hamzah –** you guys are incredible! Thanks for being there when I needed it most. **Saioa, Nagore, Gorka, Xabi, Ander, Olatz, Beg, and Lucilla,** thank you for the company during the breaks!

A mi Amama, Luz, *eres un ejemplo de angel en la tierra. Gracias por su ayuda. Tu apoyo al brindarme un espacio habitable y cómodo me ha permitido concentrarme en mi investigación y en mi familia para adaptarme al ambiente español.*

Finally, I want to dedicate this thesis to **Syahidah Rilyadi,** my wife, who has relentlessly supported me. Your unwavering belief in me has been my greatest motivation. To my loving children, **Ragnar and Mirari**, you inspire me to finish this journey with love. Thank you for your understanding, especially during those difficult times. I love you to the moon and back!

References

Almog, Y., Mavashov, A., Brusel, M., & Rubinstein, M. (2022). Functional Investigation of a Neuronal Microcircuit in the CA1 Area of the Hippocampus Reveals Synaptic Dysfunction in Dravet Syndrome Mice. *Frontiers in Molecular Neuroscience*, *15*(March), 1–17. https://doi.org/10.3389/fnmol.2022.823640

Ang, C. W., Carlson, G. C., & Coulter, D. A. (2005). Hippocampal CA1 circuitry dynamically gates direct cortical inputs preferentially at theta frequencies. *Journal of Neuroscience*, *25*(42), 9567–9580. https://doi.org/10.1523/JNEUROSCI.2992-05.2005

Anggono, V., & Huganir, R. L. (2012). Regulation of AMPA receptor trafficking and synaptic plasticity. *Current Opinion in Neurobiology*, *22*(3), 461–469. https://doi.org/10.1016/j.conb.2011.12.006

Araya, R., Vogels, T. P., & Yuste, R. (2014). Activity-dependent dendritic spine neck changes are correlated with synaptic strength. *Proceedings of the National Academy of Sciences of the United States of America*, *111*(28). https://doi.org/10.1073/pnas.1321869111

Arellano, J. I., Benavides-Piccione, R., DeFelipe, J., & Yuste, R. (2007). Ultrastructure of Dendritic Spines: Correlation Between Synaptic and Spine Morphologies. *Frontiers in Neuroscience*, *1*(1), 131–143. https://doi.org/10.3389/neuro.01.1.1.010.2007

Attardo, A., Fitzgerald, J. E., & Schnitzer, M. J. (2015). Impermanence of dendritic spines in live adult CA1 hippocampus. *Nature*, *523*(7562), 592–596. https://doi.org/10.1038/nature14467

Baer, S. M., & Rinzel, J. (1991). Propagation of dendritic spikes mediated by excitable spines: A continuum theory. *Journal of Neurophysiology*, *65*(4), 874–890. https://doi.org/10.1152/jn.1991.65.4.874

Beck, H., & Yaari, Y. (2008). Plasticity of intrinsic neuronal properties in CNS disorders. *Nature Reviews Neuroscience*, *9*(5), 357–369. https://doi.org/10.1038/nrn2371

Becker, A. J. (2018). Review: Animal models of acquired epilepsy: insights into mechanisms of human epileptogenesis. *Neuropathology and Applied Neurobiology*, *44*(1), 112–129. https://doi.org/10.1111/nan.12451

Bischofberger, J., Engel, D., Li, L., Geiger, J. R. P., & Jonas, P. (2006). Patch-clamp recording from mossy fiber terminals in hippocampal slices. *Nature Protocols*, *1*(4), 2075–2081. https://doi.org/10.1038/nprot.2006.312

Bliss, T. V. P., & Lømo, T. (1973). Long-lasting potentiation of synaptic transmission in the dentate area of the anaesthetized rabbit following stimulation of the perforant path. *The Journal of Physiology*, *232*(2), 331–356. https://doi.org/10.1113/jphysiol.1973.sp010273

Calovi, S., Soria, F. N., & Tønnesen, J. (2021). Super-resolution STED microscopy in live brain tissue. *Neurobiology of Disease*, *156*. https://doi.org/10.1016/j.nbd.2021.105420

Cavazos, J. E., & Cross, D. J. (2006). The role of synaptic reorganization in mesial temporal lobe epilepsy. *Epilepsy and Behavior*, *8*(3), 483–493. https://doi.org/10.1016/j.yebeh.2006.01.011

Clarkson, C., Smeal, R. M., Hasenoehrl, M. G., White, J. A., Rubio, M. E., & Wilcox, K. S. (2020). Ultrastructural and functional changes at the tripartite synapse during epileptogenesis in a model of temporal lobe epilepsy. *Experimental Neurology*, *326*(November 2019), 113196. https://doi.org/10.1016/j.expneurol.2020.113196

Debanne, D., Thompson, S. M., & Gähwiler, B. H. (2006). A brief period of epileptiform activity strengthens excitatory synapses in the rat hippocampus in vitro. *Epilepsia*, *47*(2), 247–256. https://doi.org/10.1111/j.1528-1167.2006.00416.x

Delgado-Sequera, A., Hidalgo-Figueroa, M., Barrera-Conde, M., Duran-Ruiz, M. ^{a}C, Castro, C., Fernández-Avilés, C., de la Torre, R., Sánchez-Gomar, I., Pérez, V., Geribaldi-Doldán, N., Robledo, P., & Berrocoso, E. (2021). Olfactory Neuroepithelium Cells from Cannabis Users Display Alterations to the Cytoskeleton and to Markers of Adhesion, Proliferation and Apoptosis. *Molecular Neurobiology*, *58*(4), 1695–1710. https://doi.org/10.1007/s12035-020-02205-9

Dyment, D. A., Schock, S. C., Deloughery, K., Tran, M. H., Ure, K., Nutter, L. M. J., Creighton, A., Yuan, J., Banderali, U., Comas, T., Baumann, E., Jezierski, A., Boycott, K. M., Mackenzie, A. E., & Martina, M. (2020). Electrophysiological alterations of pyramidal cells and interneurons of the CA1 region of the hippocampus in a novel mouse model of dravet syndrome. *Genetics*, *215*(4), 1055–1066. https://doi.org/10.1534/genetics.120.303399

Epsztein, J., Milh, M., Bihi, R. I., Jorquera, I., Ben-Ari, Y., Represa, A., & Crépel, V. (2006). Ongoing epileptiform activity in the post-ischemic hippocampus is associated with a permanent shift of the excitatory-inhibitory synaptic balance in CA3 pyramidal neurons. *Journal of Neuroscience*, *26*(26), 7082–7092. https://doi.org/10.1523/JNEUROSCI.1666-06.2006

Ergina, J. L., Amakhin, D. V., Postnikova, T. Y., Soboleva, E. B., & Zaitsev, A. V. (2021). Short-term epileptiform activity potentiates excitatory synapses but does not affect intrinsic membrane properties of pyramidal neurons in the rat hippocampus in vitro. *Biomedicines*, *9*(10). https://doi.org/10.3390/biomedicines9101374

Falco-Walter, J. (2020). Epilepsy-Definition, Classification, Pathophysiology, and Epidemiology. *Seminars in Neurology*, *40*(6), 617–623. https://doi.org/10.1055/s-0040-1718719

Fiala, J. C., Spacek, J., & Harris, K. M. (2002). Dendritic spine pathology: Cause or consequence of neurological disorders? *Brain Research Reviews*, *39*(1), 29–54. https://doi.org/10.1016/S0165-0173(02)00158-3

Galindo, L., Moreno, E., López-Armenta, F., Guinart, D., Cuenca-Royo, A., Izquierdo-Serra, M., Xicota, L., Fernandez, C., Menoyo, E., Fernández-Fernández, J. M., Benítez-King, G., Canela, E. I., Casadó, V., Pérez, V., de la Torre, R., & Robledo, P. (2018). Cannabis Users Show Enhanced Expression of CB1-5HT2A Receptor Heteromers in Olfactory Neuroepithelium Cells. *Molecular Neurobiology*, *55*(8), 6347–6361. https://doi.org/10.1007/s12035-017-0833-7

Glickfeld, L. L., & Scanziani, M. (2006). Distinct timing in the activity of cannabinoid-sensitive and cannabinoid-insensitive basket cells. *Nature Neuroscience*, *9*(6), 807–815. https://doi.org/10.1038/nn1688.Distinct

Goold, C. P., & Nicoll, R. A. (2010). Single-Cell Optogenetic Excitation Drives Homeostatic Synaptic Depression. *Neuron*, *68*(3), 512–528. https://doi.org/10.1016/j.neuron.2010.09.020

Grutzendler, J., Kasthuri, N., & Gan, W. B. (2002). Long-term dendritic spine stability in the adult cortex. *Nature*, *420*(6917), 812–816. https://doi.org/10.1038/nature01276

Gu, L., Kleiber, S., Schmid, L., Nebeling, F., Chamoun, M., Steffen, J., Wagner, J., & Fuhrmann, M. (2014). Long-term in vivo imaging of dendritic spines in the hippocampus reveals structural plasticity. *Journal of Neuroscience*, *34*(42), 13948–13953. https://doi.org/10.1523/JNEUROSCI.1464-14.2014

Guo, D., Arnspiger, S., Rensing, N. R., & Wong, M. (2012). Brief Seizures Cause Dendritic Injury. *Birth Seizures Cause Dendritic Injury*, *45*(1), 348–355. https://doi.org/10.1016/j.nbd.2011.08.020.Brief

Hablitz, J. J. (1984). Picrotoxin-induced epileptiform activity in hippocampus: Role of endogenous versus synaptic factors. *Journal of Neurophysiology*, *51*(5), 1011–1027. https://doi.org/10.1152/jn.1984.51.5.1011

Harris, K. M., Jensen, F. E., & Tsao, B. (1992). Three-dimensional structure of dendritic spines and synapses in rat hippocampus (CA1) at postnatal day 15 and adult ages. *Journal of Neuroscience*, *12*(7), 2665–2705. http://www.jneurosci.org/content/jneuro/12/7/2685.full.pdf

Hennig, M. H. (2013). Theoretical models of synaptic short term plasticity. *Frontiers in Computational Neuroscience*, *7*(APR 2013), 1–10. https://doi.org/10.3389/fncom.2013.00045

Holtmaat, A., & Svoboda, K. (2009). Experience-dependent structural synaptic plasticity in the mammalian brain. *Nature Reviews Neuroscience*, *10*(9), 647–658. https://doi.org/10.1038/nrn2699

Holtmaat, A., Wilbrecht, L., Knott, G. W., Welker, E., & Svoboda, K. (2006). Experience-dependent and cell-type-specific spine growth in the neocortex. *Nature*, *441*(7096), 979–983. https://doi.org/10.1038/nature04783

Hotulainen, P., & Hoogenraad, C. C. (2010). Actin in dendritic spines: Connecting dynamics to function. *Journal of Cell Biology*, *189*(4), 619–629. https://doi.org/10.1083/jcb.201003008

Jayant, K., Hirtz, J. J., Plante, I. J. La, Tsai, D. M., De Boer, W. D. A. M., Semonche, A., Peterka, D. S., Owen, J. S., Sahin, O., Shepard, K. L., & Yuste, R. (2017). Targeted intracellular voltage recordings from dendritic spines using quantum-dot-coated nanopipettes. *Nature Nanotechnology*, *12*(4), 335–342. https://doi.org/10.1038/nnano.2016.268

Jones, S. P., O'Neill, N., Muggeo, S., Colasante, G., Kullmann, D. M., & Lignani, G. (2022). Developmental instability of CA1 pyramidal cells in Dravet Syndrome. *BioRxiv*, 2022.09.12.507264. https://doi.org/10.1101/2022.09.12.507264

Jones, S. P., Rahimi, O., O'Boyle, M. P., Diaz, D. L., & Claiborne, B. J. (2003). Maturation of granule cell dendrites after mossy fiber arrival in hippocampal field CA3. *Hippocampus*, *13*(3), 413–427. https://doi.org/10.1002/hipo.10121

Kanemoto, Y., Matsuzaki, M., Morita, S., Hayama, T., Noguchi, J., Senda, N., Momotake, A., Arai, T., & Kasai, H. (2011). Spatial distributions of GABA receptors and local inhibition of ca 2+ transients studied with GABA uncaging in the dendrites of CA1 pyramidal neurons. *PLoS ONE*, *6*(7), 1–6. https://doi.org/10.1371/journal.pone.0022652

Klausberger, T., & Somogyi, P. (2008). Neuronal diversity and temporal dynamics: The unity of hippocampal circuit operations. *Science*, *321*(5885), 53–57. https://doi.org/10.1126/science.1149381

Kullmann, D. M. (2011). Interneuron networks in the hippocampus. *Current Opinion in Neurobiology*, *21*(5), 709–716. https://doi.org/10.1016/j.conb.2011.05.006

Kwon, T., Sakamoto, M., Peterka, D. S., & Yuste, R. (2017). Attenuation of synaptic potentials in dendritic spines Taekyung. *Cell Reports*, *20*(5), 1100–1100. https://doi.org/10.1016/j.celrep.2017.07.012.Attenuation

Levet, F., Tønnesen, J., Nägerl, U. V., & Sibarita, J. B. (2020). SpineJ: A software tool for quantitative analysis of nanoscale spine morphology. *Methods*, *174*(August 2019), 49–55. https://doi.org/10.1016/j.ymeth.2020.01.020

Liao, D., Hessler, N. A., & Mallnow, R. (1995). Activation of postsynaptically silent synapses during pairing-induced LTP in CA1 region of hippocampal slice. *Nature*, *375*(6530), 400–404.

Maillard, L., Vignal, J. P., Gavaret, M., Guye, M., Biraben, A., McGonigal, A., Chauvel, P., & Bartolomei, F. (2004). Semiologic and electrophysiologic correlations in temporal lobe seizure subtypes. *Epilepsia*, *45*(12), 1590–1599. https://doi.org/10.1111/j.0013-9580.2004.09704.x

Martín-Suárez, S., Cortes, J. M., & Bonifazi, P. (2023). Blockage of STAT3 during epileptogenesis prevents GABAergic loss and imprinting of the epileptic state. *Brain*, *146*(8), 3416–3430. https://doi.org/10.1093/brain/awad055

McKinney, R. A., Debanne, D., Gahwiller, B., & Thompson, S. M. (1997). Lesion-induced axonal sprouting and hyperexcitability in the hippocampus in vitro: implications for the genesis of posttraumatic epilepsy. *Nature Medicine*, *3*(9), 990–996. https://doi.org/10.1038/nm0798-822

Mizrahi, A., Crowley, J. C., Shtoyerman, E., & Katz, L. C. (2004). High-Resolution in Vivo Imaging of Hippocampal Dendrites and Spines. *Journal of Neuroscience*, *24*(13), 3147–3151. https://doi.org/10.1523/JNEUROSCI.5218-03.2004

Papp, E., Leinekugel, X., Henze, D. A., Lee, J., & Buzsáki, G. (2001). The apical shaft of CA1 pyramidal cells is under GABAergic interneuronal control. *Neuroscience*, *102*(4), 715–721. https://doi.org/10.1016/S0306-4522(00)00584-4

Pchitskaya, E., & Bezprozvanny, I. (2020). Dendritic Spines Shape Analysis—Classification or Clusterization? Perspective. *Frontiers in Synaptic Neuroscience*, *12*(September). https://doi.org/10.3389/fnsyn.2020.00031

Pelkey, K. A., Chittajallu, R., Craig, M. T., Tricoire, L., Wester, J. C., & McBain, C. J. (2017). Hippocampal gabaergic inhibitory interneurons. *Physiological Reviews*, *97*(4), 1619–1747. https://doi.org/10.1152/physrev.00007.2017

Penzes, P., Cahill, M. E., Jones, K. A., VanLeeuwen, J.-E., & Woolfrey, K. M. (2011). Dendritic spine pathology in neuropsychiatric disorders. *Nat Neurosci*, *14*(3), 285–293. https://doi.org/10.1038/nn.2741.Dendritic

Perez-Cruz, C., Nolte, M. W., Van Gaalen, M. M., Rustay, N. R., Termont, A., Tanghe, A., Kirchhoff, F., & Ebert, U. (2011). Reduced spine density in specific regions of CA1 pyramidal neurons in two transgenic mouse models of Alzheimer's disease. *Journal of Neuroscience*, *31*(10), 3926–3934. https://doi.org/10.1523/JNEUROSCI.6142-10.2011

Peters, A., & Kaiserman-Abramof, I. R. (1970). The small pyramidal neuron of the rat cerebral cortex. The perikaryon, dendrites and spines. *American Journal of Anatomy*, *127*(4), 321–355. https://doi.org/10.1002/aja.1001270402

Pfeiffer, T., Poll, S., Bancelin, S., Angibaud, J., Inavalli, V. V. G. K., Keppler, K., Mittag, M., Fuhrmann, M., & Nägerl, U. V. (2018). Chronic 2P-STED imaging reveals high turnover of dendritic spines in the hippocampus in vivo. *ELife*, *7*, 1–17. https://doi.org/10.7554/eLife.34700

Rakhade, S. N., Zhou, C., Aujla, P. K., Fishman, R., Sucher, N. J., & Jensen, F. E. (2008). Early alterations of AMPA receptors mediate synaptic potentiation induced by neonatal seizures. *Journal of Neuroscience*, *28*(32), 7979–7990. https://doi.org/10.1523/JNEUROSCI.1734-08.2008

Shim, H. G., Lee, Y. S., & Kim, S. J. (2018). The emerging concept of intrinsic plasticity: Activity-dependent modulation of intrinsic excitability in cerebellar Purkinje cells and motor learning. *Experimental Neurobiology*, *27*(3), 139–154. https://doi.org/10.5607/en.2018.27.3.139

Smirnova, E. Y., Amakhin, D. V., Malkin, S. L., Chizhov, A. V., & Zaitsev, A. V. (2018). Acute Changes in Electrophysiological Properties of Cortical Regular-Spiking Cells Following Seizures in a Rat Lithium–Pilocarpine Model. *Neuroscience*, *379*, 202–215. https://doi.org/10.1016/j.neuroscience.2018.03.020

Spruston, N. (2008). Pyramidal neurons: Dendritic structure and synaptic integration. *Nature Reviews Neuroscience*, *9*(3), 206–221. https://doi.org/10.1038/nrn2286

Sumi, T., & Harada, K. (2020). Mechanism underlying hippocampal long-term potentiation and depression based on competition between endocytosis and exocytosis of AMPA receptors. *Scientific Reports*, *10*(1), 1–14. https://doi.org/10.1038/s41598-020-71528-3

Swietek, B., Gupta, A., Proddutur, A., & Santhakumar, V. (2016). Immunostaining of biocytin-filled and processed sections for neurochemical markers. *Journal of Visualized Experiments*, *2016*(118), 1–9. https://doi.org/10.3791/54880

Tønnesen, J., Inavalli, V. V. G. K., & Nägerl, U. V. (2018). Super-Resolution Imaging of the Extracellular Space in Living Brain Tissue. *Cell*, *172*(5), 1108-1121.e15. https://doi.org/10.1016/j.cell.2018.02.007

Tønnesen, J., Katona, G., Rózsa, B., & Nägerl, U. V. (2014). Spine neck plasticity regulates compartmentalization of synapses. *Nature Neuroscience*, *17*(5), 678–685. https://doi.org/10.1038/nn.3682

Tønnesen, J., & Nägerl, U. V. (2013). Superresolution imaging for neuroscience. *Experimental Neurology*, *242*, 33–40. https://doi.org/10.1016/j.expneurol.2012.10.004

Tønnesen, J., & Nägerl, U. V. (2016). Dendritic spines as tunable regulators of synaptic signals. *Frontiers in Psychiatry*, *7*(JUN). https://doi.org/10.3389/fpsyt.2016.00101

Tønnesen, J., Sørensen, A. T., Deisseroth, K., Lundberg, C., & Kokaia, M. (2009). Optogenetic control of epileptiform activity. *Proceedings of the National Academy of Sciences of the United States of America*, *106*(29), 12162–12167. https://doi.org/10.1073/pnas.0901915106

Turrigiano, G. (2012). Homeostatic synaptic plasticity: Local and global mechanisms for stabilizing neuronal function. *Cold Spring Harbor Perspectives in Biology*, *4*(1), 1–17. https://doi.org/10.1101/cshperspect.a005736

Ueda, Y., Yokoyama, H., Nakajima, A., Tokumaru, J., Doi, T., & Mitsuyama, Y. (2002). Glutamate excess and free radical formation during and following kainic acid-induced status epilepticus. *Experimental Brain Research*, *147*(2), 219–226. https://doi.org/10.1007/s00221-002-1224-4

Velíšek, L. (2006). Models of Chemically-Induced Acute Seizures. *Models of Seizures and Epilepsy*, 127–152. https://doi.org/10.1016/B978-012088554-1/50013-X

Verkhratsky, A., & Nedergaard, M. (2014). Astroglial cradle in the life of the synapse. *Philosophical Transactions of the Royal Society B: Biological Sciences*, *369*(1654). https://doi.org/10.1098/rstb.2013.0595

Veruki, M. L., Mørkve, S. H., & Hartveit, E. (2003). Functional properties of spontaneous EPSCs and non-NMDA receptors in rod amacrine (AII) cells in the rat retina. *Journal of Physiology*, *549*(3), 759–774. https://doi.org/10.1113/jphysiol.2003.039982

von Bohlen und Halbach, O. (2009). Structure and function of dendritic spines within the hippocampus. *Annals of Anatomy*, *191*(6), 518–531. https://doi.org/10.1016/j.aanat.2009.08.006

Witter, M. P., Naber, P. A., Van Haeften, T., Machielsen, W. C. M., Rombouts, S. A. R. B., Barkhof, F., Scheltens, P., & Lopes Da Silva, F. H. (2000). Cortico-hippocampal communication by way of parallel parahippocampal-subicular pathways. *Hippocampus*, *10*(4), 398–410. https://doi.org/10.1002/1098-1063(2000)10:4<398::AID-HIPO6>3.0.CO;2-K

Wong, M., & Guo, D. (2013). Dendritic spine pathology in epilepsy: Cause or consequence? *Neuroscience*, *251*, 141–150. https://doi.org/10.1016/j.neuroscience.2012.03.048

Yuste, R., & Bonhoeffer, T. (2001). Morphological changes in dendritic spines associated with long-term synaptic plasticity. *Annual Review of Neuroscience*, *24*(1862), 1071–1089. https://doi.org/10.1146/annurev.neuro.24.1.1071

Zeng, L. H., Xu, L., Rensing, N. R., Sinatra, P. M., Rothman, S. M., & Wong, M. (2007). Kainate seizures cause acute dendritic injury and actin depolymerization in vivo. *Journal of Neuroscience*, *27*(43), 11604–11613. https://doi.org/10.1523/JNEUROSCI.0983-07.2007

Zha, X. M., Green, S. H., & Dailey, M. E. (2005). Regulation of hippocampal synapse remodeling by epileptiform activity. *Molecular and Cellular Neuroscience*, *29*(4), 494–506. https://doi.org/10.1016/j.mcn.2005.04.007

Zucker, R. S., & Regehr, W. G. (2002). Short-term synaptic plasticity. *Annual Review of Physiology*, *64*, 355–405. https://doi.org/10.1146/annurev.physiol.64.092501.114547